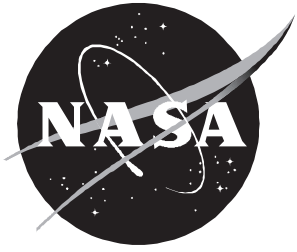


Predicting Radiative Heat Transfer in Thermochemical Nonequilibrium Flow Fields

Theory and User's Manual for the LORAN Code

Lin Hartung Chambers



Predicting Radiative Heat Transfer in Thermochemical Nonequilibrium Flow Fields

Theory and User's Manual for the LORAN Code

Lin Hartung Chambers
Langley Research Center • Hampton, Virginia

The use of trademarks or names of manufacturers in this report is for accurate reporting and does not constitute an official endorsement, either expressed or implied, of such products or manufacturers by the National Aeronautics and Space Administration.

Acknowledgment

The assistance of Robert A. Mitcheltree in establishing the LAURA code interface is gratefully acknowledged.

This publication is available from the following sources:

NASA Center for AeroSpace Information
800 Elkridge Landing Road
Linthicum Heights, MD 21090-2934
(301) 621-0390

National Technical Information Service (NTIS)
5285 Port Royal Road
Springfield, VA 22161-2171
(703) 487-4650

Contents

Nomenclature	v
Preface	ix
THEORY	1
1. Radiation Theory	1
1.1. Atomic Mechanisms	2
1.1.1. Bound-Bound Transitions	2
1.1.2. Bound-Free Transitions	4
1.1.3. Free-Free Transitions	6
1.2. Molecular Mechanisms	6
1.3. Induced Emission	7
2. Electronic Excitation Theory	8
3. Transport Theory	11
3.1. Plane-Parallel Medium	11
3.2. Multidimensional Medium	13
4. Flow-Field Coupling	13
PRACTICE	14
5. Implementation	14
5.1. Initial Setup	15
5.1.1. Data Input	15
5.1.2. Flow-Field Data	15
5.1.3. Maximum Rotational Quantum Number	16
5.1.4. Continuum Spectrum	16
5.2. Radiation Properties	18
5.2.1. Bound-Bound Transitions	18
5.2.2. Bound-Free Transitions	19
5.2.3. Free-Free Transitions	19
5.2.4. Molecular Transitions	19
5.3. Radiative Transport	20
5.3.1. Numerical Solution	20
5.3.2. Special Case for Constant τ_ν	22
5.4. Flow-Field Coupling	22
6. Computational Optimization	24
6.1. Radiation Calculation	24
6.2. Excitation Calculation	24
6.3. Radiation Subgrid	24

7. Using the Code	25
7.1. Include Files	26
7.2. Input Files	26
7.3. Output Files	26
8. Conclusions	27
Appendix A—Gaussian Units	28
Appendix B—Molecular Radiation Model	29
Appendix C—Code Structure	39
Appendix D—Input Guide	41
Appendix E—Tecplot File Format	61
References	62

Nomenclature

A	transition probability, sec^{-1}
a_0	Bohr radius, cm
B	rotational constant, eV
B_{lu}	Einstein coefficient for absorption
b	normalized line shape, sec
c	speed of light, cm/sec
D	dissociation energy from ground state, eV
D_{el}	matrix element, statcoulomb-cm
D_v	second rotational constant, eV
d_q	under-relaxation constant
E	energy or energy level, eV
e	electron charge, statcoulomb
F	normalized line shape
f	distribution function
f_{lu}	oscillator strength for line transitions
g	degeneracy
H	heavy-particle impact excitation rate, $\text{cm}^3\text{-sec}^{-1}$
h	Planck's constant, eV-sec or erg-sec
$h\nu$	energy, eV
I	ionization potential of ground state, eV
I_ν	radiative intensity, $\text{W}/\text{cm}^2\text{-sec}^{-1}\text{-sr}$
J	rotational quantum number
J^e	total line emission, W/cm^3
j_ν^e	emission coefficient, $\text{W}/\text{cm}^3\text{-sec}^{-1}\text{-sr}$
j_ν^l	induced emission coefficient, $\text{W}/\text{cm}^3\text{-sec}^{-1}\text{-sr}$
K	electron impact excitation rate, $\text{cm}^3\text{-sec}^{-1}$
k	Boltzmann's constant, eV/K or erg/K; normal grid point
M	reaction partner
m	mass, g
N	number density, cm^{-3}
n	principal quantum number
n_c	number of captures per unit volume per unit time
p	rotational transition probability
Q	partition function

q	Franck-Condon factor
\mathbf{q}_R	radiative flux, W/cm^2
r_e	intermolecular distance, \AA
s	path variable, cm
T	temperature, K
u_ν	radiation density
v	vibrational quantum number
v	speed, cm/sec
W	weighting factor in subgrid algorithm
Z	ion charge number
Z_k	radiation subgrid weighting function
z	normal coordinate, cm
α	correction to rotational constant, eV
α_e	spectroscopic constant, eV
β	correction to second rotational constant, eV
γ	line half-width at half-maximum, sec^{-1}
η	wall normal coordinate, cm
κ	absorption coefficient, cm^{-1}
κ'	absorption coefficient corrected for induced emission, cm^{-1}
λ	wavelength, cm
μ	cosine of angle between $\hat{\Omega}$ and Z -axis
ν	frequency, sec^{-1}
Σ	molecular state designator
σ	cross-section, cm^2
τ	optical variable
$\hat{\Omega}$	direction vector
ω_e	spectroscopic constant, eV
$\omega_e x_e$	spectroscopic constant, eV
$\omega_e y_e$	spectroscopic constant, eV
$\omega_e z_e$	spectroscopic constant, eV
Subscripts:	
A	lower electronic state of molecule
a	perturbing atoms
B	upper electronic state of molecule
CL	line center

c	capture or continuum
e	electron
el	electronic
h	heavy particle
i	index of energy level
J^u, J^l	rotational quantum number
j	index of energy level
k	grid index in Z direction
l	lower state of radiative transition
max	maximum
min	minimum
n	index of electronic level
P	$\Delta J = -1$ rotational transition
p	Planck function
Q	$\Delta J = 0$ rotational transition
R	$\Delta J = 1$ rotational transition
R	radiative
r	rotational
s	species index
t	translational
tot	total
u	upper state of radiative transition
V	vibrational-electron-electronic
v	vibrational
w	wall
z	z component or derivative
0	reference
ν	frequency
+	ion
∞	free stream
Superscripts:	
D	Doppler profile
e	emission
el	electronic
L	Lorentz profile

<i>l</i>	lower state
<i>n</i>	index of time step in iteration
<i>R</i>	resonance
<i>S</i>	Stark profile
<i>u</i>	upper state
*	photoionization threshold
<i>l</i>	integration dummy variable
<i>''</i>	integration dummy variable
-	negative <i>Y</i> direction
+	positive <i>Y</i> direction

Abbreviations:

CFD	computational fluid dynamics
HWHM	half-width at half-maximum
LAURA	Langley Aerothermodynamic Upwind Relaxation Algorithm
LORAN	Langley Optimized RAdiative Nonequilibrium
NBS	National Bureau of Standards

Preface

In recent years, proposals for lunar and Mars missions have proliferated. A common feature of many of these proposals is a large aerobrake that would engender significant radiative heating during the atmospheric pass. These large aerobrakes are intended to perform their maneuvers at high altitude; therefore, the flow may be in thermochemical nonequilibrium for all or at least a significant part of the trajectory. Existing equilibrium radiative heating codes are not well suited to this problem. Existing nonequilibrium radiative heating codes have been considered either too costly (NEQAIR, ref. 1) or too approximate (Viscous Shock Layer, RAD/EQUIL, ref. 2) for use in coupled solutions of this type of flow field.

The objective of this work is to describe a new method for efficiently predicting thermal radiation effects on vehicles flying through the rarefied upper layers of the atmosphere where thermochemical nonequilibrium flow occurs.

The Langley Optimized RAdiative Nonequilibrium (LORAN) code was developed for this purpose. The LORAN code includes atomic bound-bound, bound-free, and free-free transitions as well as molecular band radiation. Radiative cooling effects can be treated if the LORAN code is coupled with a flow-field code. The Langley Aerothermodynamic Upwind Relaxation Algorithm (LAURA) code was used for that purpose in the development of LORAN. To achieve an efficient computation, spectral approximations and optimization are introduced and controlled by a few parameters in the code. To further reduce computation time, a radiation subgrid is selected.

This user's manual presents a review of the theory on which the LORAN code is based and is followed by a practical discussion of the implementation in a FORTRAN code. Descriptions of the input and output files and the run-time options are also provided. The manual should benefit both the occasional user of the LORAN code and those who wish to use it as a starting point for further modeling enhancements.

Part of the information presented in this report was included in a thesis entitled "Nonequilibrium Radiative Heating Prediction Method for Aeroassist Flowfields with Coupling to Flowfield Solvers" submitted by Lin C. Hartung in partial fulfillment of the requirements for the Degree of Doctor of Philosophy in Aerospace Engineering, North Carolina State University, Raleigh, North Carolina, April 1991.

THEORY

1. Radiation Theory

Predicting the emission and absorption of thermal radiation in a gas involves computing the transitions between various energy levels in the atoms and molecules. The resulting complete spectral variation of emission and absorption is contained in the absorption coefficient κ_ν and the emission coefficient j_ν^e . The absorption coefficient is obtained from the product of the population density N_n of energy level n and its radiation absorption cross section $\sigma_{\nu n}$, summed over all the energy levels available. Thus,

$$\kappa_\nu = \sum_l N_l \sigma_{\nu l} \quad (1)$$

where l is the absorbing levels. The spontaneous emission coefficient is found from a similar expression in which the amount of energy emitted $h\nu_{ul}$ also appears, and the absorption cross section is replaced by the transition probability for emission A_{ul} in which u and l denote the upper and lower energy levels, respectively. Thus,

$$J^e = \sum_u N_u \sum_l h\nu_{ul} A_{ul} \quad (2)$$

where u is the emitting levels. These expressions and the remainder of the development in this section are written for a single species to simplify the notation. For a gas mixture such as air, properties are computed for each species and are added to obtain the mixture properties (i.e., $\kappa_\nu = \sum_s \kappa_{\nu,s}$).

In equilibrium gases, the electronic energy-level populations are determined as a function of a uniquely defined equilibrium temperature according to a Boltzmann distribution. The rotational and vibrational energy levels of each electronic state of a molecule are populated according to the equilibrium partition function. Equilibrium relations exist between species concentrations. All these equilibrium equations allow radiative properties to be referenced to temperature and to the concentrations of a few major species, thereby allowing the development of simple radiation step models. Also, under equilibrium conditions, the absorption and emission coefficients are related according to Kirchhoff's law, so that equation (2) is not needed.

In nonequilibrium gases, these simple relations for the energy-state populations and species concentrations no longer apply. The problem now is to determine the nonequilibrium populations of each energy level. The rotational and vibrational states in a molecule may be assumed populated according to distinct rotational and vibrational temperatures T_r and T_v , respectively, if the excitation/de-excitation mechanisms among the states of these energy modes are fast enough. If these mechanisms are not effectively instantaneous with respect to the time scales of the flow, further separation of energy modes is required. Generally, T_r and T_v adequately describe the respective energy modes in most hypersonic flows. The electronic states, however, being more widely separated, equilibrate more slowly, so that a single electronic temperature may be a bad assumption, even within a single species. In this situation the electronic energy-level populations in the absorption and emission coefficients must be calculated individually at every spatial and frequency point according to the specific local conditions. The emission coefficient cannot be calculated from the Kirchhoff relation between absorption and emission. The radiative cross sections, however, depend only on the configuration of an individual atom or molecule and are the same for equilibrium and nonequilibrium conditions. The necessary expressions for the nonequilibrium absorption and emission coefficients of the various radiative transitions are developed below without employing equilibrium relations.

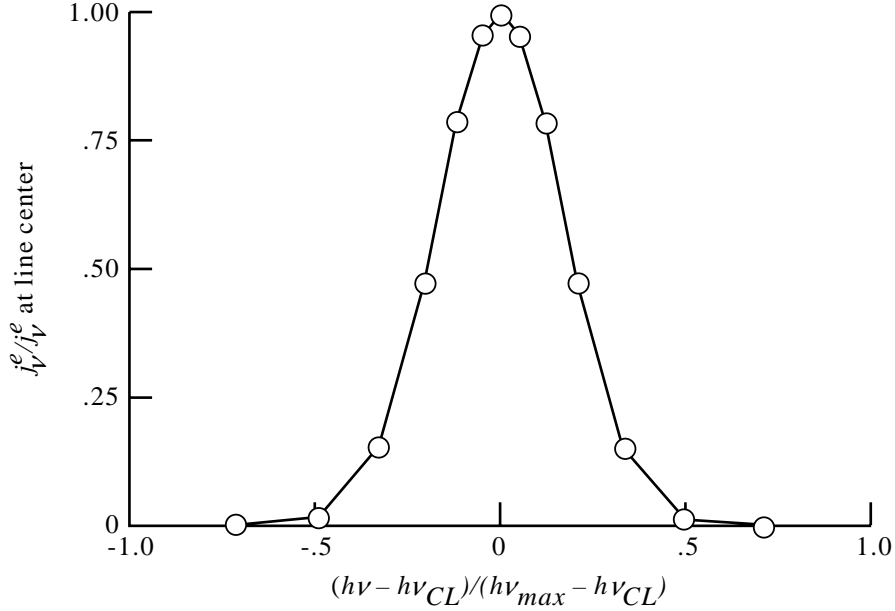


Figure 1. Distribution of spectral points for atomic line.

Most radiation work has historically been done in the Gaussian system of units. This system introduces the particular oddity of measuring the electron charge in statcoulombs. As this particular unit of measure is not commonly used in engineering, some of what follows may be confusing. To clarify the situation, relevant information on the Gaussian system is provided in appendix A.

1.1. Atomic Mechanisms

Atomic radiation involves transitions of electrons in bound or free states of an atom. Computing the radiation from atomic mechanisms requires knowledge of the energy levels of each atomic species. Many electronic energy levels occur in a typical atom and these must be modeled by a manageable set of inputs. To reduce bookkeeping and complexity, a common practice is to group neighboring energy levels into one lumped level along with an appropriate overall degeneracy. This practice has been adopted here. The grouped levels from the Park quasi-steady-state (QSS) method (ref. 1) are used for nitrogen and oxygen atoms (22 levels for atomic nitrogen, 19 levels for atomic oxygen), yielding values for the principal quantum number n and the energy level E_n for each level.

1.1.1. Bound-Bound Transitions

Bound-bound or atomic line transitions are those between bound electronic levels of atomic species. The method used in the present study for computing bound-bound transitions is adapted from that developed by Nicolet (ref. 2) for the RAD/EQUIL code. This model resolves an atomic line by distributing an odd number of spectral points starting from the line center as shown in figure 1. Following the Nicolet development, with modifications required for nonequilibrium, the absorption coefficient in a line is given by

$$\kappa_\nu = \frac{\pi e^2}{mc} f_{lu} N_l b(\nu, N_e, T_t, T_e, \dots) \quad (3)$$

where f_{lu} is the oscillator strength of the transition, N_l is the population density of the lower state of the transition, and b is the line shape function that may depend on many variables. The constants e , m , and c are the electron charge, electron mass, and speed of light, respectively.

The line shape is a normalized function that can be described by one of several theoretical models depending on the predominant broadening mechanism. The Lorentz shape describes lines in which Stark broadening by electron impact dominates, as is often the case for heavy atomic species. This line shape is given as

$$b_\nu = \frac{\gamma^S/\pi}{(\nu - \nu_{CL})^2 + (\gamma^S)^2} \quad (4)$$

where the dependence of b on the gas conditions has been omitted. Here, γ^S is the Stark half-width at half-maximum (HWHM) and ν_{CL} is the frequency of the line center. The HWHM is the half-width of the line at half its height, a common descriptor for line shapes.

Stark HWHM's have been calculated by various authors, most notably Griem. (See ref. 3.) Page et al. (ref. 4) noted that these line widths vary with a power n of the electron kinetic temperature T_e as

$$\gamma^S(T_e) \approx \left(\frac{T_e}{T_0}\right)^n \gamma^S(T_0) = \left(\frac{T_e}{T_0}\right)^n \gamma_0^S(T_0) N_e \quad (5)$$

thus allowing use of a single input reference for Stark broadening γ_0^S , which is the HWHM per electron at the reference temperature T_0 (10 000 K here). The assumption of a linear dependence on the electron number density N_e is implicit in equation (5) and follows reference 5. The values of γ_0^S and n for the important lines treated in the LORAN code are included in the input files.

The mechanism of resonance broadening yields Lorentz line shapes as well. This mechanism may exceed Stark broadening for situations with low ionization. Resonance broadening occurs when radiating and perturbing particles are of the same type and uncharged (so Stark broadening does not occur). When the perturbers have the same natural frequency as the radiators, a resonance effect produces strong coupling between them and results in a wider frequency spread (i.e., resonance broadening). This effect is important only when sufficient particles are in the appropriate initial state, generally when the initial state has a low-lying energy level. The RAD/EQUIL code, in fact, included this contribution only for a few lines with low-lying lower states. For completeness in nonequilibrium heating, the LORAN code computes it for all lines. Hunt and Sibulkin (ref. 5) give the approximate HWHM as¹

$$\gamma^R \approx 3\pi \left(\frac{g_l}{g_u}\right)^{1/2} \left(\frac{e^2 f_{lu}^R}{2\pi m \nu^R}\right) N_a \quad (6)$$

where N_a is the number of perturbing atoms per unit volume (i.e., the number of atoms in the lower state of the line transition) and g_l and g_u are the degeneracies of the lower and upper states, respectively. The effective Lorentz line width is the sum of γ^S and γ^R . (See ref. 6.)

The second line shape is the Doppler profile, which describes line broadening due to thermal motion of the atoms. This Gaussian line shape is given as

$$b_\nu = \frac{1}{\gamma^D} \sqrt{\frac{\ln 2}{\pi}} \exp\left[-\frac{(\nu - \nu_{CL})^2 \ln 2}{(\gamma^D)^2}\right] \quad (7)$$

¹ The 1/2 power on g_l/g_u was omitted in Nicolet. (See ref. 2.) Also note that the RAD/EQUIL code contains an extra g_l factor, which results from a different treatment of N_a .

The Doppler HWHM is given by

$$\gamma^D = \frac{\nu_{CL}}{c} \sqrt{\frac{2kT_t \ln 2}{m_s}} \quad (8)$$

where k is Boltzmann's constant and m_s is the mass of the radiating species s . The temperature is the heavy-particle translational temperature T_t that is due to the thermal motion of the atoms.

The Lorentz and Doppler line shapes are different, so that these two line widths cannot simply be added. Convolution leads to a Voigt line shape combining the two types of effects but requiring significantly more computation. Faster approximations to the Voigt line shape have been developed in recent years. The LORAN code applies an approximation developed by Whiting (ref. 7) if this additional accuracy is desired. This approximation gives the Voigt profile within 5 percent everywhere. The Voigt line width is computed from γ^L and γ^D according to reference 8. If more approximate results are acceptable, both Lorentz and Doppler line shapes are computed, and the largest of b^L and b^D at each frequency point is used.

After the appropriate line shape is calculated at each spatial grid point, the absorption coefficient in a line can be computed from equation (3) and from input data for the oscillator strength and line width and the predicted nonequilibrium energy-level populations.

The total radiative emission from an atomic line into all directions (ref. 9) is given by

$$J_{ul}^e = N_u h \nu_{ul} A_{ul} \quad (9)$$

where A_{ul} is the Einstein coefficient for spontaneous emission of the transition from the upper atomic energy level u to the lower level l . Detailed balancing relates A_{ul} to the absorption oscillator strength f_{lu} (ref. 9) as follows:

$$A_{ul} = \frac{8\pi^2 e^2}{mc^3} \frac{g_l}{g_u} \nu_{ul}^2 f_{lu} \quad (10)$$

Combining these two equations leads to the spectral emission coefficient for bound-bound atomic transitions (now per steradian). The line shape b is the same as that for absorption.

$$j_\nu^e = \frac{2\pi h e^2}{mc^3} \frac{g_l}{g_u} \nu_{ul}^3 f_{lu} N_u b(\nu, N_e, T_t, T_e, \dots) \quad (11)$$

When the electronic state populations are in equilibrium, the expressions for the bound-bound absorption and emission coefficients satisfy Kirchhoff's law, the appropriate limiting form.

1.1.2. Bound-Free Transitions

Atomic bound-free or photoionization transitions involve a bound electron being detached from an atom by an incoming photon or the reverse process of radiative electron capture. A model for bound-free transitions can be developed by assuming a hydrogen-like atom. A good source of such a development for an equilibrium gas is Zeldovich and Raizer. (See ref. 9, ch. 5, sec. 5.) The radiative cross sections developed there also apply to nonequilibrium because the configuration of an atom in a particular excited state is unchanged whether the gas around it is in equilibrium or nonequilibrium. From that reference, therefore, the cross section for an atomic energy level n is

$$\sigma_{\nu n} = \frac{1}{\sqrt{3}} \frac{32\pi^4 m Z^4 e^{10} Q_+^{\text{el}}}{3\nu^3 c h^6 n^3 g_n} \quad (12)$$

where Z is the charge number ($Z = 1$ for neutral species) and h is Planck's constant. Note that in this expression the electronic partition function of the ion has not been assumed equal to 1, as was done in reference 9. Further, the degeneracy has not been replaced in the denominator by using the hydrogenic model. For grouped or lumped electronic levels, the hydrogenic model does not correctly describe the degeneracy.

Once the cross section is obtained, the spectral absorption coefficient can be computed for the bound-free process, given the nonequilibrium populations of the electronic energy levels of the atom. The relation is

$$\kappa_\nu = \sum_{n^*}^{\infty} N_n \sigma_{\nu n} \quad (13)$$

The lower limit n^* indicates the photoionization threshold and is the lowest atomic energy level from which a photon of frequency ν can detach an electron. The upper limit in practice has a finite value corresponding to ionization of the atom.

Although quite accurate, equation (12) can be improved further. In particular, a correction from quantum mechanics (ref. 9, p. 266), sometimes called a Gaunt factor, may be applied to it. The approximate factor developed by Biberman (ref. 10) for low-energy photons has been applied here. Although only an average correction that was derived for thermal equilibrium conditions, the approximate factor nevertheless provides reasonable results for the flow-field conditions examined so far. More detailed Gaunt factors may be available from other sources which apply better to nonequilibrium flows. However, these factors require substantially more work for a marginal improvement in the results because the order of magnitude of the correction does not change. Therefore, inclusion of such detailed Gaunt factors has been deferred.

Also significant is the error in this expression for low quantum states near the ground atomic state where the hydrogen-like assumption is invalid. For many atoms, the cross section of the ground state is well-known from experimental data. This information is used for transitions involving the ground state instead of the value predicted by equation (12).

Bound-free emission results from the capture of a free electron into an ion. The cross section for this process is given by Zeldovich and Raizer (ref. 9) as

$$\sigma_{cn} = \frac{128\pi^4}{3\sqrt{3}} \frac{Z^4 e^{10}}{mc^3 h^4 v^2 n^3 \nu} \quad (14)$$

where v is the initial speed of the captured electron. The number n_c of such captures into the n th energy level for electrons with speeds between v and $v + dv$ per unit volume per unit time is

$$n_c = N_+ N_e f(v) dv v \sigma_{cn} \quad (15)$$

The electron speeds follow the distribution function $f(v)$, which is assumed to be a Maxwell distribution in equilibrium at the electron translational temperature T_e . (The validity of this assumption in a plasma with Debye effects may be a candidate for further investigation.) The energy emitted $h\nu_{ul}$, where the subscript u now denotes the free state, is given by the sum of the initial kinetic energy of the electron and the net energy required to reionize it from the final energy level l .

$$h\nu_{ul} = \frac{mv^2}{2} + (I - E_l) \quad (16)$$

where I is the ground-state ionization potential and E_l is the energy of the bound level and is measured from the ground atomic state. This equation is solved for v^2 and substituted to eliminate v in favor of the frequency ν in equations (14) and (15).

After these pieces are combined, the emission coefficient for bound-free transitions is found from

$$j_\nu^e d\nu = \sum_l \frac{1}{4\pi} h\nu_{ul} n_c d\nu \quad (17)$$

where l is now the final levels. The complete expression is

$$j_\nu^e = \frac{128\pi^4}{3\sqrt{3}} \frac{Z^4 e^{10}}{m^2 c^3 h^2} N_+ N_e \left(\frac{m}{2\pi k T_e} \right)^{3/2} \sum_{n_{\min}}^{n_{\max}} \frac{1}{n^3} \exp[-(h\nu - I + E_l)/kT_e] \quad (18)$$

The lower limit on the summation corresponds to capture of a zero-energy electron; n_{\min} is determined for each frequency by setting ν to zero in equation (16). The upper limit is determined by ionization of the atom. A quantum correction to this result is needed as discussed above. The Gaunt factor used for emission is identical to that for absorption.

When the electronic state populations are in equilibrium with the free electrons, the nonequilibrium absorption and emission coefficients developed here for bound-free transitions satisfy Kirchhoff's law, as required.

1.1.3. Free-Free Transitions

Atomic free-free transitions, also called bremsstrahlung radiation, result when a free electron passing near a heavy particle is decelerated and gives off energy in the form of radiation. Such radiation cannot occur in electron-electron collisions because momentum and energy cannot both be conserved. (See ref. 6, p. 137.) In fact, only transitions due to a nearby atomic ion are considered here. Free-free transitions caused by neutral atoms and molecules are assumed to be negligible because the cross sections are generally one or two orders of magnitude less. (See ref. 9, p. 256.) A model for free-free transitions can also be developed using semiclassical methods. Zeldovich and Raizer (ref. 9, ch. 5, sec. 3) is again a good source. The result they obtained can be rederived without using equilibrium assumptions except for a Maxwell distribution of the energies of the free electrons at T_e . In this case, the only change in the result is that T_e replaces T . The equation for the free-free absorption coefficient can therefore be written as

$$\kappa_\nu = \frac{4}{3} \left(\frac{2\pi}{3mkT_e} \right)^{1/2} \frac{Z^2 e^6}{hcm\nu^3} N_+ N_e \quad (19)$$

where N_+ is the concentration of the appropriate ion. This result could also be modified by a quantum correction, but the effect is minimal for the conditions in typical hypersonic flow fields.

Free-free transitions are a special case in nonequilibrium gases because they involve only free electrons (the effect on the energy of the ion is negligible). Free electrons are assumed to equilibrate rapidly to some T_e ; thus, Kirchhoff's law and the development of the emission coefficient lead to the same result,

$$j_\nu^e = \frac{8}{3} \left(\frac{2\pi}{3mkT_e} \right)^{1/2} \frac{Z^2 e^6}{mc^3} N_+ N_e \exp(-h\nu/kT_e) \quad (20)$$

so that as $T_e \rightarrow T$, the equilibrium values will be recovered.

1.2. Molecular Mechanisms

The treatment of molecular radiation requires consideration of vibrational and rotational transitions within the molecule as well as electronic transitions and combinations of the different

types of transition. Each such transition contributes a discrete line to the radiation spectrum whose line center frequency is determined by the energy differential of the transition. A line-by-line calculation of molecular radiation is possible, but it does not fit the requirements of the present study for a relatively rapid calculation method which can be coupled to a flow-field code. As an alternative, therefore, the ‘‘smeared band’’ model of molecular radiation is used. In this model, the rotational line structure of the molecular radiation is smoothed to provide a continuous variation of the absorption coefficient. Because the rotational energy levels are so closely spaced, the lines resulting from rotational transitions are nearly overlapping except in rarefied conditions. The error introduced by this approximation should therefore be acceptable under most conditions of interest. However, if the LORAN code is applied to a new gas regime, this assumption should be checked.

The basic development of the smeared-band model can be found in several sources. (See refs. 9, 11, and 12.) The development given in appendix B is an enhancement of that found in Zeldovich and Raizer. (See ref. 9, ch. 5, sec. 3.) It incorporates higher order expressions for the molecular energy levels from Herzberg (ref. 13), while eliminating equilibrium assumptions.

The final result for the smeared-band molecular absorption coefficient $\bar{\kappa}$ is

$$\begin{aligned} \bar{\kappa}_{\nu AB} = & \frac{8\pi^3}{3hc} \frac{1}{g_A} D_{elBA}^2 \sum_{v^l}^{\infty} \sum_{v^u}^{\infty} \frac{q_{v^u v^l}}{\lambda} \sum_{j^l}^{\infty} \frac{N_A}{Q_v(T_v)} \frac{\exp(-E_{v^l}/kT_v)}{|B_{v^u} - B_{v^l}| Q_r(T_r)} \\ & \times \exp\left(-hc \left\{ \left[B_e^l - \alpha_e^l \left(v^l + \frac{1}{2} \right) \right] \left(\frac{1}{\lambda} - \frac{1}{\lambda_{v^u v^l}} \right) \frac{1}{B_{v^u} - B_{v^l}} \right. \right. \\ & \left. \left. - \frac{4B_e^{l3}}{\omega_e^{l2}} \left(\frac{1}{\lambda} - \frac{1}{\lambda_{v^u v^l}} \right)^2 \frac{1}{(B_{v^u} - B_{v^l})^2} \right\} / kT_r \right) \end{aligned} \quad (21)$$

The emission coefficient is given by

$$\begin{aligned} \bar{j}_{\nu AB}^e = & \frac{16\pi^3}{3g_B c^2} D_{elBA}^2 \sum_{v^u}^{\infty} \sum_{v^l}^{\infty} q_{v^u v^l} \frac{c^3}{\lambda^4} \sum_{j^u}^{\infty} \frac{N_B}{Q_v(T_v)} \frac{\exp(-E_{v^u}/kT_v)}{|B_{v^u} - B_{v^l}| Q_r(T_r)} \\ & \times \exp\left(-hc \left\{ \left[B_e^u - \alpha_e^u \left(v^u + \frac{1}{2} \right) \right] \left(\frac{1}{\lambda} - \frac{1}{\lambda_{v^u v^l}} \right) \frac{1}{B_{v^u} - B_{v^l}} \right. \right. \\ & \left. \left. - \frac{4B_e^{u3}}{\omega_e^{u2}} \left(\frac{1}{\lambda} - \frac{1}{\lambda_{v^u v^l}} \right)^2 \frac{1}{(B_{v^u} - B_{v^l})^2} \right\} / kT_r \right) \end{aligned} \quad (22)$$

These expressions give the smeared absorption and emission coefficients for all rotational and vibrational levels in a given transition from lower electronic state A to upper electronic state B .

1.3. Induced Emission

The above expressions for the emission coefficient do not include all the radiation emitted by the medium. Stimulated or induced emission also occurs when photons are present. This emission is proportional to the radiative intensity I_ν and is, therefore, commonly included as a correction to the absorption coefficient. The induced emission (ref. 9, ch. 2, sec. 4) is given by

$$j_\nu^i = j_\nu^e \frac{c^2}{2h\nu^3} I_\nu \quad (23)$$

In equilibrium gases, I_ν in equation (23) becomes the Planck black-body function, and the usual result from Kirchhoff's law is obtained. In nonequilibrium gases, the intensity cannot be replaced with the Planck function. Instead, the induced emission coefficient of equation (23) must be substituted in the transport equation along with the coefficients for spontaneous emission and absorption. The transport equation then becomes

$$\frac{\partial I_\nu(s, \hat{\Omega})}{\partial s} + \kappa_\nu(s) I_\nu(s, \hat{\Omega}) = j_\nu^e(s) + j_\nu'(s) \quad (24)$$

where j_ν^e is the spontaneous emission coefficient and $\hat{\Omega}$ is the direction. (See sec. 6.) Substituting equation (23) and gathering terms containing I_ν then allows the definition of a corrected absorption coefficient for thermochemical nonequilibrium equal to the factor that multiplies I_ν . The result is

$$\kappa_\nu' = \kappa_\nu - j_\nu^e \frac{c^2}{2h\nu^3} \quad (25)$$

The corrected absorption coefficient κ_ν' may be negative in nonequilibrium. Negative values occur when the nonequilibrium populations are such that the second term on the right of equation (25) is larger than the first term. Physically, this negative κ_ν' means that the upper energy level of a transition or transitions is overpopulated relative to the lower energy level. Such a population inversion can occur in a nonequilibrium boundary layer, for instance, when the higher energy levels are still populated according to the temperature and chemistry of the inviscid shock layer. This fact must be carefully considered when developing any solution algorithm for radiative transport in nonequilibrium problems. Because of the term $1/\nu^3$ in equation (25), negative values of κ_ν' generally occur at the low-energy end of the spectrum.

2. Electronic Excitation Theory

The electronic states of atoms and molecules in a gas can become perturbed through many excitation mechanisms and reactions. In equilibrium gases, these effects balance, so that the states are populated according to a Boltzmann distribution. To obtain the nonequilibrium electronic-level population densities N_i for the i th electronic state of each atomic and molecular species in a gas, rate equations must be written for each level (of each species), including all possible populating and depopulating mechanisms.

The populating mechanisms are as follows:

1. Electron impact excitation or de-excitation from bound state j to bound state i :



2. Heavy particle impact excitation or de-excitation from bound state j to bound state i :



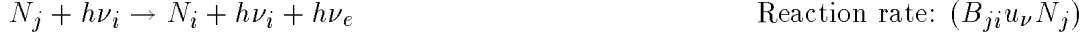
3. Radiative absorption in lower bound state j transitioning to higher bound state i :



4. Spontaneous radiative emission from higher bound state j decaying to lower bound state i :



5. Induced radiative emission from higher bound state j decaying to lower bound state i :



6. Collisional deionization from free state c to bound state i :



7. Radiative deionization from free state c to bound state i :

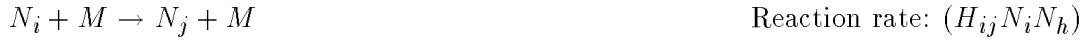


The corresponding depopulating mechanisms are as follows:

1. Electron impact de-excitation or excitation from bound state i to bound state j :



2. Heavy particle impact de-excitation or excitation from bound state i to bound state j :



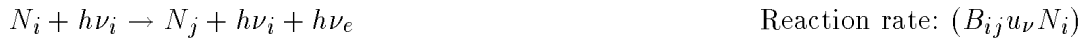
3. Radiative absorption in lower bound state i into higher bound state j :



4. Spontaneous radiative emission from higher bound state i to lower bound state j :



5. Induced radiative emission from higher bound state i to lower bound state j :



6. Collisional ionization from bound state i to free state c :



7. Radiative ionization from bound state i to free state c :



The rate of change of the population density N_i in a control volume can be written

$$\frac{\partial N_i}{\partial t} = \dot{N}_i^{\text{in}} - \dot{N}_i^{\text{out}} - \nabla \cdot (N_i \mathbf{v}_i) \quad (26)$$

where the first term on the right denotes the creation of N_i through the first seven mechanisms above, the second term is the removal of N_i due to the corresponding depopulation mechanisms,

and the last term represents the net flux of N_i across the boundaries of the control volume. The velocity \mathbf{v}_i is the effective velocity of the particles in the i th electronic level of species s . The source and sink terms can be written explicitly in terms of the above mechanisms as

$$\begin{aligned} \dot{N}_i^{\text{in}} = & \sum_{j=1}^{j_{\text{max}}} K_{ji} N_j N_e + \sum_{j=1}^{j_{\text{max}}} H_{ji} N_j N_h + \sum_{j=1}^{i-1} B_{ji} u_\nu N_j + \sum_{j=i+1}^{j_{\text{max}}} A_{ji} N_j \\ & + \sum_{j=i+1}^{j_{\text{max}}} B_{ji} u_\nu N_j + K_{ci} N_+ N_e^2 + A_{ci} N_+ N_e \end{aligned} \quad (27)$$

$$\begin{aligned} \dot{N}_i^{\text{out}} = & \sum_{j=1}^{j_{\text{max}}} K_{ij} N_i N_e + \sum_{j=1}^{j_{\text{max}}} H_{ij} N_i N_h + \sum_{j=i+1}^{j_{\text{max}}} B_{ij} u_\nu N_i + \sum_{j=1}^{i-1} A_{ij} N_i \\ & + \sum_{j=1}^{i-1} B_{ij} u_\nu N_i + K_{ic} N_i N_e + A_{ic} u_\nu N_i \end{aligned} \quad (28)$$

To solve for the population densities, data on the various rates of excitation and de-excitation of each level are required. Radiative transition rates are reasonably well known. Collisional rates are more elusive. Sources for such data are varied, and the rates presented are often uncertain due to the experimental difficulties involved in the measurements. Park (ref. 1) has collected a comprehensive set of rates for nitrogen and oxygen species. He cites the uncertainty in the data set as a factor of 2 and asserts that the impact on the excited-state populations is negligible. This set has been adopted here; however, further verification of this accuracy would be desirable in the future.

Equation (26) is not usually solved as is. Rather, the usual approximation is to assume a quasi-steady-state (QSS) distribution of excited states. The QSS model assumes that the rate of change in a population is small compared with the rate of transitions into and out of that level (ref. 14, ch. 3); that is,

$$\left| \frac{\partial N_i}{\partial t} \right| \ll \dot{N}_i^{\text{in}} \quad (29)$$

$$\left| \frac{\partial N_i}{\partial t} \right| \ll \dot{N}_i^{\text{out}} \quad (30)$$

If the divergence term $\nabla \cdot (N_i \mathbf{v}_i)$ is also negligible, then equation (26) reduces to

$$\dot{N}_i^{\text{in}} - \dot{N}_i^{\text{out}} \approx 0 \quad (31)$$

or

$$\frac{dN_i}{dt} \approx 0 \quad (32)$$

and thus is transformed from a set of differential equations to a set of algebraic equations. This method is designed for use when the amount of nonequilibrium is “not too large,” such that the assumptions above are reasonable. In particular, the present application does not account for the history of the flow in areas of high gradients (boundary layer and shock), where $\nabla \cdot (N_i \mathbf{v}_i)$ is not necessarily negligible. Effectively, this approach decouples the excitation from the macroscopic flow-field solution.

The QSS assumption requires that the relaxation time be much less than the dwell time in the flow and is best satisfied for upper excited states in which the atoms and molecules transition rapidly back and forth to the free state. However, because QSS in effect predicts instantaneous accommodation to the local conditions, it will rise faster in the shock and fall faster in the boundary layer. The integrated effect on radiative flux to the wall, for example, may be quite accurate.

A further difficulty arises in this equation because the radiative absorption and induced emission terms depend on the incident radiation in the form of radiation density u_ν , which is not known a priori. A rigorous solution for the excited-state populations would require complete coupling of the radiative, excitation, and chemical processes in the flow, which is not yet feasible because of computational limitations and lack of rate data. An alternative would be an iterative process in which QSS populations without radiation are used to compute radiation, and the result is then fed back into equation (26) until the iteration converges. This process is formidable and computationally expensive, however. Instead, approximations are normally invoked. The simplest approximation is to assume that absorption and induced emission do not affect the QSS populations (optically thin assumption). This assumption is not accurate if ultraviolet lines are considered, although induced emission can usually be neglected. To account for radiative absorption, a radiation escape factor can be defined. (See refs. 14–16.) This approach is an approximate and somewhat empirical means of correcting the populations for absorption effects. It allows the limits on population levels to be determined by computing them with full absorption and no absorption. The escape factor is used here, based on an approximate flow dimension which the user must supply. The solution to the QSS equation proceeds according to the methods developed by Park in the NEQAIR code. (See ref. 1.)

3. Transport Theory

The complete equation of radiative transport has been derived in many standard texts. Neglecting transients and assuming a nonscattering medium, it simplifies to

$$\frac{dI_\nu(s, \hat{\Omega})}{ds} + \kappa'_\nu(s)I_\nu(s, \hat{\Omega}) = j_\nu^e(s) \quad (33)$$

However, neglecting scattering may not be valid for ultraviolet radiation in O_2 , for example; and scattering must be included to treat ablating flows.

For some frequencies, κ'_ν can be negative in part of a nonequilibrium flow (sec. 1.3), so it may pass through zero somewhere in the domain. Therefore, the usual procedure of dividing by κ'_ν to transform this equation to an optical variable would introduce a singularity. For this work, then, equation (33) is left in terms of the physical coordinate.

Equation (33) applies at each ν and for each $\hat{\Omega}$. A formal solution can be written using an integrating factor. The radiative transport can then be computed numerically for a finite number of frequency points and directions. A method of selecting appropriate frequencies at which to compute the radiative properties j_ν^e and κ'_ν in a nonequilibrium flow is discussed in sections 5 and 6. Approximate methods for dealing with the directional variations are discussed next.

3.1. Plane-Parallel Medium

A common approximation for solving the radiative transport equation is to assume that the properties of the medium through which the radiation travels vary in only one direction. This situation is illustrated by the inset in figure 2 and may be a reasonable assumption in the

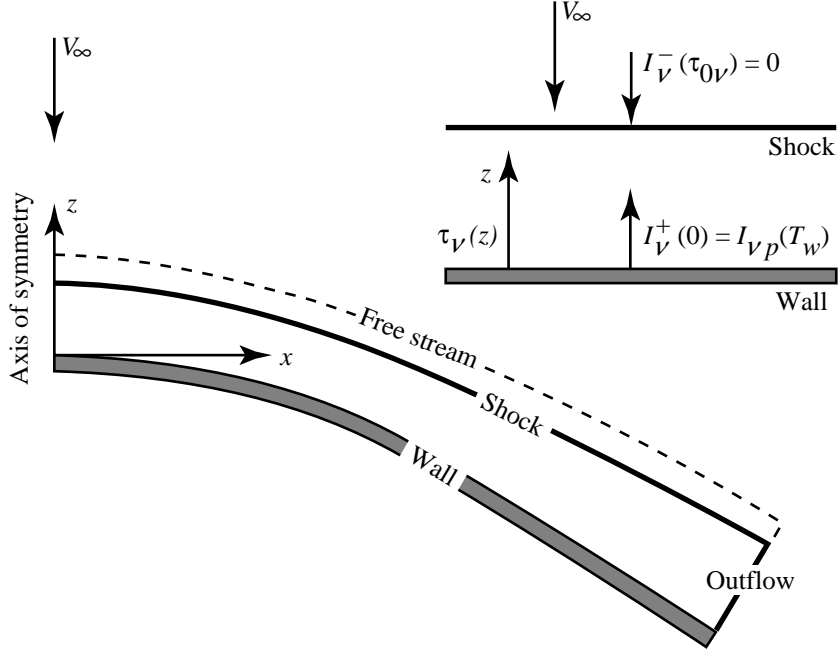


Figure 2. Flow geometry and radiation boundary conditions.

stagnation region of a flow field, where gradients are mainly in the normal direction. In this case s and $\hat{\Omega}$ are replaced by z and μ (the cosine of the angle between $\hat{\Omega}$ and the z -axis). The derivative d/ds then becomes $\mu\partial/\partial z$. To accommodate the boundary conditions in this case, I_ν is split into forward ($\mu > 0$) and backward ($\mu \leq 0$) components. The formal solution for each can be written as

$$\begin{aligned}
 I_\nu^+(z, \mu) &= I_\nu^+(0, \mu) \exp\left\{-\int_0^z \left[\frac{\kappa_\nu^l(s'', \mu)}{\mu}\right] ds''\right\} \\
 &+ \int_0^z \left(\frac{j_\nu^e(s', \mu)}{\mu} \exp\left\{-\int_{s'}^z \left[\frac{\kappa_\nu^l(s'', \mu)}{\mu}\right] ds''\right\}\right) ds'
 \end{aligned} \tag{34}$$

$$\begin{aligned}
 I_\nu^-(z, \mu) &= I_\nu^-(z_0, \mu) \exp\left\{-\int_{z_0}^z \left[\frac{\kappa_\nu^l(s'', \mu)}{\mu}\right] ds''\right\} \\
 &+ \int_{z_0}^z \left(\frac{j_\nu^e(s', \mu)}{\mu} \exp\left\{-\int_{s'}^z \left[\frac{\kappa_\nu^l(s'', \mu)}{\mu}\right] ds''\right\}\right) ds'
 \end{aligned} \tag{35}$$

The boundary $z = 0$ is the vehicle surface, which is assumed to emit radiation according to Planck's function at the imposed wall temperature T_w . The boundary $z = z_0$ is the free-stream gas ahead of the vehicle, which is assumed not to emit radiation. The equations for the geometry along the normal to the wall ($\mu = \pm 1$) are

$$I_\nu^+(z, 1) = I_{\nu p}(T_w) e^{-\tau_\nu(z)} + \int_0^z j_\nu^e(s') e^{\tau_\nu(s') - \tau_\nu(z)} ds' \tag{36}$$

$$I_\nu^-(z, -1) = \int_z^{z_0} j_\nu^e(s') e^{\tau_\nu(z) - \tau_\nu(s')} ds' \tag{37}$$

where τ_ν is the optical variable (introduced without division by 0 in equation (33)):

$$\tau_\nu(z) = \int_0^z \kappa'_\nu(s') ds' \quad (38)$$

To obtain the radiative flux in an absorbing, plane-parallel medium, the formal solutions above for the intensity must be integrated over all directions. If azimuthally symmetric radiation is assumed and if the exponential approximation is employed to replace the exponential integral functions (refs. 2 and 17), the result is

$$\mathbf{q}_{\nu R}(z) = \pi \left[I_{\nu p}(T_w) e^{-2\tau_\nu(z)} + 2 \int_0^z j'_\nu(s') e^{2\tau_\nu(s') - 2\tau_\nu(z)} ds' - 2 \int_z^{z_0} j'_\nu(s') e^{2\tau_\nu(z) - 2\tau_\nu(s')} ds' \right] \quad (39)$$

Although this approach involves an approximation, it provides excellent results (within 10 percent for a typical blunt body) compared with the exact integration over the direction of the incoming intensity.

The divergence of the radiative flux is obtained by differentiating equation (39) with respect to z , then integrating over the complete spectral range. The differentiation can be done analytically or numerically from the solution for $\mathbf{q}_{\nu R}(z)$. The latter approach has been implemented here and follows that of Nicolet. (See ref. 2.) The analytical approach requires a numerical differentiation of the integrand and would be similarly accurate.

To obtain the total radiative flux, the spectral radiation is integrated over frequency:

$$\mathbf{q}_R(z) = \int_{\nu_1}^{\nu_2} \mathbf{q}_{\nu R}(z) d\nu \quad (40)$$

The theoretical limits on the spectral integration are $\nu_1 = 0$ and $\nu_2 = \infty$. In practice, finite limits are required and are included as inputs to the computer code. The lower limit is often set around 0.3 eV because a zero-energy photon causes a singularity in the free-free absorption coefficient. (See eq. (19).) The singularity arises because additional quantum mechanical considerations not discussed here must be included at very low energies. The radiative energy omitted by ignoring these low-energy transitions is minimal. Most gas radiation in shock layers in air occurs at energies below 16.5 eV, which is a typical upper limit. An alternate upper limit at 6.2 eV includes only the visible and infrared portions of the spectrum. This range of energies is easier to measure experimentally and includes minimal self-absorption, but it is not sufficient if coupling effects are of interest.

3.2. Multidimensional Medium

When the tangent slab approximation is invalid, the directional variation of the radiation must be accounted for. Because an exact solution of the radiative transport equations in multidimensional media is not feasible, an approximate method is needed. One such method is described in reference 18. This method appears as an option in the LORAN code, but the interested reader is referred to that reference for more details because the transport method is still being developed. Overall, the required inputs and the resulting output are the same for either transport method.

4. Flow-Field Coupling

Radiation is inherently coupled to the state of the gas from which it emanates and results from radiative transitions in the internal energy states of the atoms, molecules, and ions in the gas.

The radiation emitted by such transitions travels through the gas at the speed of light until it is reabsorbed or exits the flow field. Radiation thus provides an additional energy transport mode. Radiation can also affect the chemical state of the gas through photodissociation, photoionization, and radiative recombination.

Energy transport through the gas by radiation is modeled in the Navier-Stokes equations with a term that appears in the energy equation: the divergence of the radiative flux $\nabla \cdot \mathbf{q}_R$ (denoted Q_{rad} by Gnoffo, Gupta, and Shinn in ref. 19). This divergence term is computed in the LORAN radiation-transport model. When the tangent slab approximation is used, $\nabla \cdot \mathbf{q}_R = d\mathbf{q}_R/d\eta$. The radiation effects on chemical kinetics can be included by adding photoreactions to the chemistry model of the gas and accounting for their effects on radiation properties. The radiation effects on chemical kinetics are not included in the current LAURA and LORAN codes.

Energy transport due to radiation is usually neglected in the aerothermodynamic analysis of hypersonic flow fields. For flow fields in which this assumption is not valid, the effects of radiation can be determined by comparing solutions from calculations with and without radiative energy transport. In general, the shock layer becomes nonadiabatic when radiation transport is included. The enthalpy of a parcel of fluid decreases due to radiative cooling as it traverses the layer from the shock to the boundary layer edge. For equilibrium gas calculations, the temperature profiles decrease across the shock layer as a result. Lower average temperatures result in higher average densities and thus decreased shock standoff distance. The combination of lower temperatures and a thinner shock layer reduces the radiative heat load to the wall. In the boundary layer, however, a net absorption of radiation may occur, leading to locally increased temperature and enthalpy and to a possible increase in convective heating.

In a thermochemical nonequilibrium gas calculation, multiple temperatures are defined to describe the partitioning of energy across the internal modes. The number of temperatures required to adequately describe the flow depends on the conditions. For example, rotational, vibrational, and electronic energy modes for the mixture or for each species may be used. The various states of each energy mode are assumed to be in equilibrium at the characteristic temperature of that mode. Each mode is described by its own energy conservation equation, which includes terms coupling it to the other energy modes. Usually, separate internal modes for each species are not defined because the energy modes are assumed strongly coupled between species.

To correctly model the radiative coupling in the nonequilibrium case, only that portion of $\nabla \cdot \mathbf{q}_R$ associated with transitions of each particular energy mode should be included in the energy equation for that mode. Purely rotational radiative transitions occur at low infrared energies—which are generally neglected in gas radiation—so all radiative transitions of interest in air are assumed to involve a transition between vibrational and/or electronic states. The LAURA code currently employs the two-temperature model. (See ref. 20.) This model is implemented with two energy equations: a total energy equation (for total temperature T_t) and a combined vibrational-electron-electronic energy equation (for the temperature T_V). Thus, because the complete $\nabla \cdot \mathbf{q}_R$ contains no pure rotational transitions, it appears in both energy equations.

PRACTICE

5. Implementation

The implementation in a practical computer code of the theory for radiation transitions and radiative transport developed in the section entitled “Theory” requires some additional work. The details of the process are described below.

The present method is implemented in the LORAN code, which was developed using two existing codes as starting points. The RAD/EQUIL program (ref. 21) was followed in developing

some of the code structure. It also is the source of part of the algorithm used to model atomic line radiation. Significant changes have been made, however, to remove equilibrium assumptions. The QSS excitation portion of the NEQAIR program (ref. 1) has been minimally adapted for use in the LORAN code.

The LORAN code is divided into four major sections: reading data and setting up properties which are constant for a calculation (including the optimized spectral array), calculating the nonequilibrium excitation, evaluating the radiative properties, and solving the radiative transport problem. The excitation calculation is from the well-known NEQAIR code; therefore, it will not be discussed in this section.

5.1. Initial Setup

5.1.1. Data Input

To evaluate the expressions for absorption and emission obtained in section 1 for each radiating mechanism, input values are required. Data are also required to predict the nonequilibrium populations of the various bound energy levels; also, flow-field data are required to define the local gas conditions. Finally, program control inputs are desirable to maximize the flexibility of the method without requiring constant reprogramming and recompiling. These inputs should allow the user to turn individual radiating mechanisms or species on or off to perform detailed studies of the radiation spectrum. They should also provide for selection of options in the code (i.e., equilibrium vs. QSS populations, flux vs. intensity, etc). The inputs are obtained from various sources, as discussed below. Most of the inputs are species properties and will not change unless significantly different new data become available.

5.1.2. Flow-Field Data

The information required about the gas conditions consists of the number densities of each radiating species considered and the temperatures for the several energy modes. The LAURA flow-field solver (ref. 22) is the source of the flow-field data used in developing this method. It is an 11-species model which provides number densities for all the nitrogen/oxygen radiating species of interest. The LAURA code currently incorporates a two-temperature model for thermal nonequilibrium. (See ref. 20.) The rotational and heavy-particle translational energy modes are assumed equilibrated, whereas the vibrational, electronic, and electron translational energy modes are assumed in equilibrium with each other but not necessarily with the other modes. Thus, the separate T_v and T_e carried in the development of the absorption and emission coefficients are equal, as are T_r and T_t . The distinction between these temperatures was maintained in the LORAN code, however, so that each can be used if the separate temperatures become available from the LAURA code or from another CFD code in the future. Some recent work (ref. 23) suggests further that distinct vibrational temperatures may exist for each molecular species. Should a CFD code ever include such detail, minor modifications to the LORAN code will allow these individual values of T_v to be used.

An effort has been made to keep the input of the flow-field properties from the LAURA code generic so that, with minor changes to a single driver routine, the LORAN code can be interfaced with a different CFD code. In fact, a few cases have already been run with flow-field data obtained from the RAD/EQUIL code (ref. 2), a direct simulation Monte Carlo code (ref. 24), and a four-temperature CFD code. (See ref. 25.) Coupled solutions have been obtained with the LAURA and GIANTS codes. (See ref. 26.)

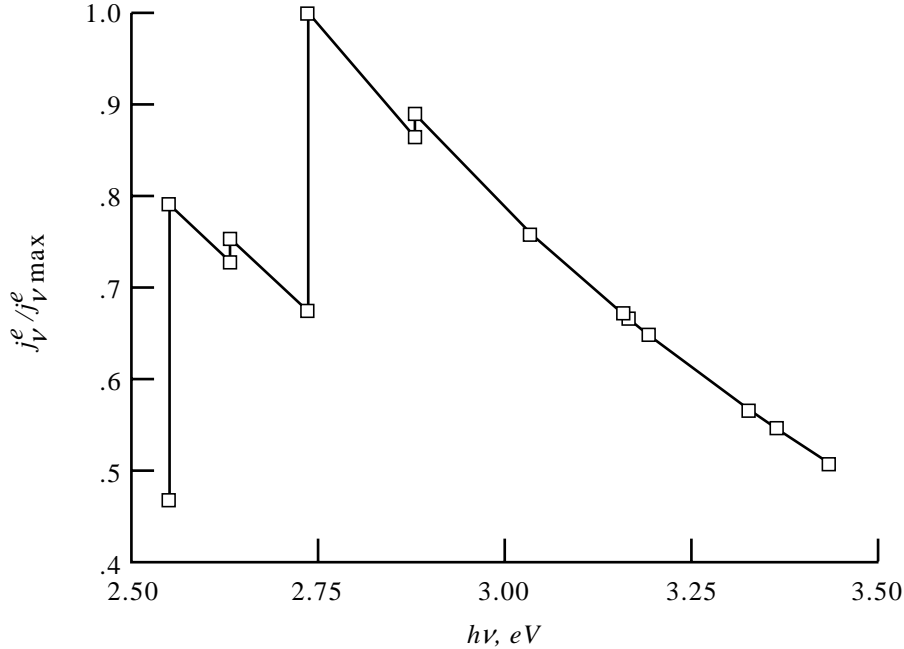


Figure 3. Example of spectrum optimization for bound-free continuum.

5.1.3. Maximum Rotational Quantum Number

The radiative property data discussed above are read into the program first. As part of this process, the maximum rotational quantum numbers are assessed using the algorithm developed by Whiting. (See sec. B.2.) These values do not change in the program.

5.1.4. Continuum Spectrum

The spectral location of all radiating transitions is determined from the set of energy levels in the atoms and molecules appearing in the gas. This information can be used to select a minimum set of spectral points for use in the radiation calculation.

Consider the bound-free continuum. The absorption coefficient for this mechanism is a smooth function of frequency with discontinuities known as photoionization edges that correspond to the activation of additional energy levels. To resolve this spectrum, spectral points must be placed within a small interval on either side of each jump, as shown in figure 3. However, this interval is much smaller than needed for the smooth portions of the curve. The RAD/EQUIL code took advantage of this fact by allowing the user to input a few spectral points to capture the jumps. In the LORAN code, this procedure is automated and incorporated in the radiation calculation. For the particular set of atomic species considered in a computation, a tailored atomic spectrum is generated to resolve the active discontinuities, as the figure illustrates. This tailoring simplifies the inputs and eliminates the chances of omitting a level. It also allows the atomic continuum calculation (including the smooth free-free continuum) to be performed on the minimum resolving array of spectral points.

As discussed in section 1, the molecular radiation has been modeled here using the smeared band approximation that smoothes the rotational structure into an exponential variation. To resolve the resulting spectrum, spectral points must be placed around each vibrational band head. A few points are sufficient to capture the smoothed rotational variation within each such band. The resulting structure is similar to the bound-free spectrum, although it is much more complicated because the vibrational bands are far more numerous and often overlap. These

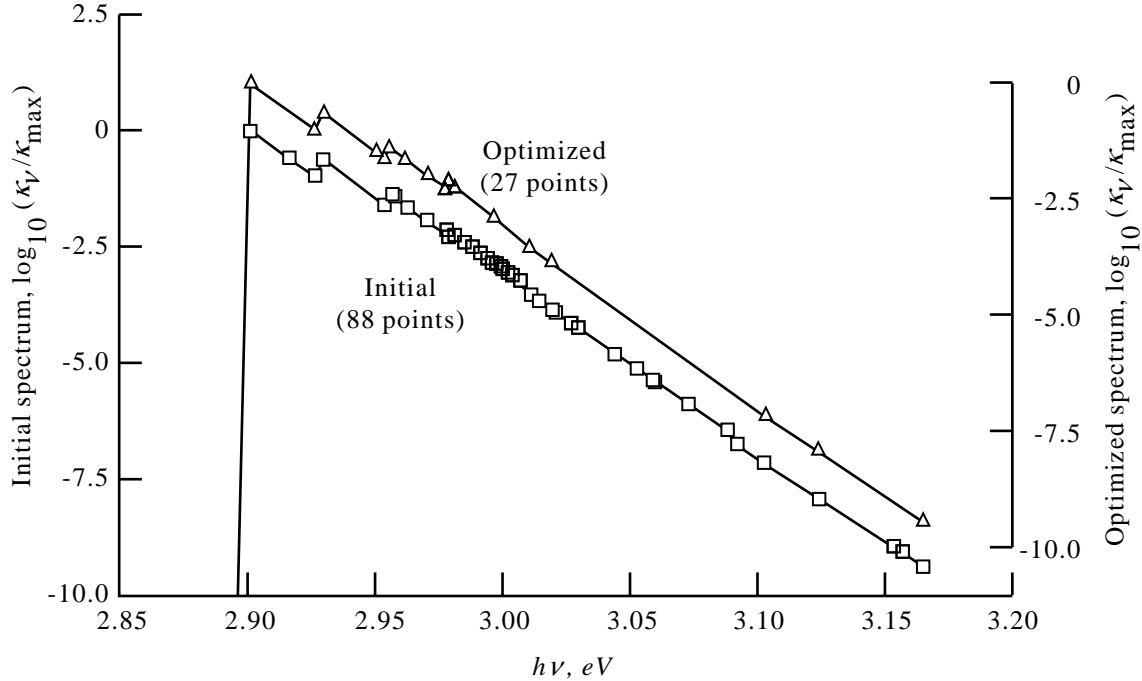


Figure 4. Example of spectrum optimization for vibrational band of electronic transition.

considerations have been used to develop an algorithm to choose an optimal molecular spectrum for each input spectral range and set of active species as follows:

1. For each active species, the vibrational band heads in the spectral range studied are computed from equation (88) with $J = 0$.
2. An initial spectrum is generated by resolving the band head and spacing nv points in the interval between $J = 0$ and the maximum rotational level ($J = J_{\max}$). An example for a major vibrational band of N_2^+ is given by the initial spectrum in figure 4. Note that the clustering of points along this curve results from additional weaker bands which underlie this major band.
3. The absorption coefficient decreases rapidly for a given vibrational band (note the log scale in fig. 4) so this spectrum can be reduced. This reduction is done by discarding points that describe a vibrational band away from its band head (points required to resolve the jump are kept), if they are within a given interval *crit* (a FORTRAN variable) of another point. This procedure can reduce the spectral array by nearly an order of magnitude.
4. A second reduction can be made by discarding any point with a neighbor within a smaller interval *crit2*.

Application of these steps to the spectrum in figure 4 results in the optimized spectrum shown. Application to the entire set of vibrational bands permits a spectrum that resolves the molecular transitions with less than 5000 points and that is optimized for any species and spectral range. This calculation sifts through many possible spectral points to produce the optimized molecular spectrum. It is computationally expensive so it is exercised only once per run. The resulting spectrum is stored for all further computations. Appropriate selection of the parameters nv , *crit*, and *crit2* controls the amount of detail included in the molecular spectrum and its size.

After a complete optimized spectrum is obtained, the index of the first and last spectral points for each vibrational band is determined. These indexes simplify the logic required in computing the molecular band radiation and improve the calculation efficiency.

About 50 points from the optimized molecular spectrum that resolve strong vibrational transitions are identified and interleaved into the atomic continuum spectrum discussed above. The resulting spectrum of about 150 points is referred to as the modified atomic spectrum and is discussed in section 5.3.

5.2. Radiation Properties

5.2.1. Bound-Bound Transitions

The oscillator strengths f_{lu} , line centers ν_{CL} , and Stark HWHM's γ_0^S are needed to compute the bound-bound transitions. The National Bureau of Standards (NBS) has published many line centers and oscillator strengths (ref. 27); the Stark HWHM information is available from Griem (ref. 3) among others. In addition, the energy levels and degeneracies of the upper and lower transition levels are in the NBS compilation. The set of inputs currently used in the LORAN code is modified from the atomic line inputs of Park's NEQAIR code. In addition, for those lines for which the HWHM is not known, an approximate correlation by Park is used. (See ref. 28.)

In the RAD/EQUIL code, Nicolet approximated the so-called high-series lines by an integral. These lines have lower state quantum numbers of four or greater, are numerous, and are closely spaced below 3.2 eV. Park treats each of these lines individually in the NEQAIR code. In the present method, to reduce the number of lines computed and therefore the run time, the high-series lines are represented by multiplet-averaged values. Data for these averaged lines are obtained from the NBS tables for transitions corresponding to Park's inputs. The line width of each averaged line is then multiplied by an appropriate factor to account for the nearly identical closely spaced lines it represents. Integration under this larger wavelength gives the total emission and absorption for the multiplet, but transport is calculated for only one line. This approximation should have minimal impact on the results, yet it halves the number of lines that must be treated.

The line shape models for the LORAN code are adapted from the development by Nicolet (ref. 2) as implemented in the RAD/EQUIL code. (See ref. 21.) Each line is resolved by a small number $nppl$ (generally less than or about 15 to 21) of spectral points that are distributed starting from the line center. (See fig. 1.) The location of the spectral point farthest from the line center is determined from the broadened width of each atomic line and the distance to the nearest neighbor. Line-broadening mechanisms treated include Doppler, resonance, and Stark, as discussed in section 1. Lorentz and Doppler line shapes are both computed and the larger of b^L and b^D is used at each spectral point in a line. If required, additional accuracy is obtained from an approximation to the Voigt line shape, combining Lorentz and Doppler effects, which is accurate to about 5 percent.

In Nicolet's implementation, the line width used to distribute the $nppl$ points was an approximation to the maximum width in the gas layer so that all or most of the energy in each line would be included. This approximate maximum width was calculated at a location input by the user at which the maximum temperature was expected. For an application in which a complete flow field is to be computed, the identification of a maximum line width presents some difficulties. Further, because the line width may vary by orders of magnitude between various points in a flow field, the use of a spectrum geared to the largest width can result in significant loss of accuracy. For these reasons, the routine which sets up the line frequency spectrum (subroutine `freq` of RAD/EQUIL) has been modified for application to every point in the flow field. This modification results in the specification of a local set of spectral points based on the local line width. These disparate frequency spectra are then reconciled to generate a single atomic line spectrum. This process results in the selection of a set of spectral points capturing the energy in a line at its broadest but that involves detailed spectral information

at each grid point. This technique allows satisfactory resolution of the atomic lines without requiring excessive storage or computation.

An additional change made to Nicolet’s method arises because Stark broadening is not always the dominant effect on line width. In the original RAD/EQUIL code, the point distribution logic in subroutine `freq` considered only the Stark line width. In the present model, the larger of the Doppler or Lorentz (Stark-effect) line width is used. Although this change is small, it should result in more complete coverage of the atomic line radiation in the present model.

The RAD/EQUIL code has also been modified to use nonequilibrium excited state populations and electron temperature, where appropriate. The Doppler line width remains a function of heavy-particle temperature because it arises from the thermal motion of the atoms themselves.

5.2.2. Bound-Free Transitions

The bound-free photoionization edge structure, which is the characteristic shape for this mechanism, is produced by the activation of each level in the summation term of equation (13). This summation requires determining the lowest accessible bound energy level n^* for each spectral energy point in the atomic continuum spectrum and summing the radiation properties for n^* and all levels above it to the ionization limit. The ground-state cross sections are invoked as constants to avoid the errors arising from the hydrogenic model, as discussed in section 1. Each atomic energy level is treated individually in the bound-free calculation but, because these are grouped levels, many more energy levels are in fact approximated and included. Gaunt factors are applied to the computation by table lookup of the Biberman and Norman correction factor. (See ref. 10.)

5.2.3. Free-Free Transitions

The free-free contribution is computed on the same spectrum as the bound-free radiation. The resolution thus obtained is more than sufficient and allows the two atomic continuum processes to be easily combined. However, because of its form (eqs. (19) and (20)), free-free radiation is significant only at low energies.

5.2.4. Molecular Transitions

To predict the molecular band radiation, spectroscopic constants must be provided that describe the distribution of rotational and vibrational energy levels. These constants are in numerous sources, such as Herzberg (ref. 13); Bond, Watson, and Welch (ref. 6); and many others. These sources also provide the necessary information on the electronic energy levels and energy-level degeneracies in molecules. The intensity of radiation depends on the Franck-Condon factors $q_{v'v''l}$ and on the electronic transition moments D_{elBA} . Data on these quantities may be found in many, often contradictory sources. The complete set of molecular inputs collected by Park for his NEQAIR code (ref. 1) has been adopted here for simplicity.

The molecular band radiation is computed with the optimized molecular spectrum the determination of which was discussed in section 5.1. The expressions for the emission and absorption coefficients developed in section 4.1 have many terms in common. Advantage is taken of these common terms to reduce the computation time. The molecular calculation remains one of the more expensive parts of the radiation calculation, so care was taken in programming this particular mechanism to ensure that the advantages of vectorization are exploited to the extent possible.

5.3. Radiative Transport

The radiative transport calculation employs an approximate treatment of atomic lines based on the RAD/EQUIL method. A single mean value of the continuum (atomic continuum plus molecular band) absorption and emission coefficient is computed for each line and added to the detailed line-only absorption and emission coefficients calculated at the *nppl* points that describe the line. These mean values are obtained by interpolating the information in the optimized continuum spectra, thus avoiding an expensive computation at each of the *nppl* spectral points that describe a line. Each atomic line covers only a very small part of the spectrum, so this approximation should be fairly accurate. Radiative transport is then computed at all *nppl* spectral points. This detailed result can be integrated over frequency to provide an average flux for each line if a concise presentation is desired, or it can be presented in full detail.

The molecular spectrum can be averaged to obtain values at each point in the much smaller modified atomic continuum spectrum, so that the number of spectral points for which transport must be calculated is significantly reduced. Because these approximate results are based on a detailed molecular spectrum of both emission and absorption, the prediction of molecular radiation transport should be quite accurate.

5.3.1. Numerical Solution

The integrals in equations (36)–(38) require some care. Because κ'_ν can be negative in some regions, the log-linear variation assumed by Nicolet (ref. 2) in the RAD/EQUIL code cannot be used. Examination of κ'_ν profiles suggests that a piecewise linear approximation is acceptable. For the optical variable, then, the integral is evaluated on the discrete grid as follows:

$$\tau_\nu(z_n) = \int_0^{z_n} \kappa'_\nu(s') ds' \approx \sum_{k=1}^{n-1} \int_{z_k}^{z_{k+1}} \kappa'_\nu(s') ds' \quad (41)$$

For this simple integral, a piecewise linear variation of κ'_ν is easily shown to lead to the following result:

$$\tau_\nu(z_n) \approx \frac{1}{2} \sum_{k=1}^{n-1} [\kappa'_\nu(z_k) + \kappa'_\nu(z_{k+1})](z_{k+1} - z_k) \quad (42)$$

For the intensity integrals, the flow-field grid spacing may be such that for strongly absorbing spectral regions, Δz is large with respect to variations in the integrand, particularly because of the exponential terms. To integrate accurately, examination of τ_ν profiles suggests that a piecewise linear approximation again should be used. By setting $\tau_\nu(s) = a_k s + b_k$ in each grid interval and by approximating j_ν^e based on the average of its values at the two ends of the interval, the integral over the exponential term can be carried out analytically. (The obvious approach of also setting $j_\nu^e = c_k s + d_k$ causes numerical problems for low values of τ_ν resulting from terms which go to 0/0.) On the discrete grid, the integrals are developed as follows:

$$I_\nu^+(z_n, 1) = I_{\nu p}(T_w) e^{-\tau_\nu(z_n)} + \sum_{k=1}^{n-1} \frac{1}{2} [j_\nu^e(z_k) + j_\nu^e(z_{k+1})] e^{-\tau_\nu(z_n)} \int_{z_k}^{z_{k+1}} e^{a_k s' + b_k} ds' \quad (43)$$

$$I_\nu^-(z_n, -1) = \sum_{k=n}^{k_{\max}-1} \frac{1}{2} [j_\nu^e(z_k) + j_\nu^e(z_{k+1})] e^{\tau_\nu(z_n)} \int_{z_k}^{z_{k+1}} e^{-a_k s' - b_k} ds' \quad (44)$$

The two integrals remaining in this equation are of a similar form and can be evaluated for general A_k and B_k as follows:

$$\begin{aligned}
\int_{z_k}^{z_{k+1}} e^{A_k x + B_k} dx &= e^{B_k} \int_{z_k}^{z_{k+1}} e^{A_k x} dx \\
&= e^{B_k} \frac{e^{A_k x}}{A_k} \Big|_{z_k}^{z_{k+1}} \\
&= \frac{e^{B_k}}{A_k} \left(e^{A_k z_{k+1}} - e^{A_k z_k} \right) \\
&= \frac{1}{A_k} \left(e^{A_k z_{k+1} + B_k} - e^{A_k z_k + B_k} \right) \tag{45}
\end{aligned}$$

Substituting this result into the integrals in equations (43) and (44), we get

$$I_\nu^+(z_n, 1) = I_{\nu p}(T_w) e^{-\tau_\nu(z_n)} + \sum_{k=1}^{n-1} \frac{1}{2} [j_\nu^e(z_k) + j_\nu^e(z_{k+1})] e^{-\tau_\nu(z_n)} \frac{1}{a_k} \left(e^{a_k z_{k+1} + b_k} - e^{a_k z_k + b_k} \right) \tag{46}$$

$$I_\nu^-(z_n, -1) = \sum_{k=n}^{k_{\max}-1} \frac{1}{2} [j_\nu^e(z_k) + j_\nu^e(z_{k+1})] e^{\tau_\nu(z_n)} \frac{1}{-a_k} \left(e^{-a_k z_{k+1} - b_k} - e^{-a_k z_k - b_k} \right) \tag{47}$$

This expression can be rephrased in terms of the optical variable as

$$I_\nu^+(z_n, 1) = I_{\nu p}(T_w) e^{-\tau_\nu(z_n)} + \sum_{k=1}^{n-1} \frac{1}{2a_k} [j_\nu^e(z_k) + j_\nu^e(z_{k+1})] e^{-\tau_\nu(z_n)} \left[e^{\tau_\nu(z_{k+1})} - e^{\tau_\nu(z_k)} \right] \tag{48}$$

$$I_\nu^-(z_n, -1) = - \sum_{k=n}^{k_{\max}-1} \frac{1}{2a_k} [j_\nu^e(z_k) + j_\nu^e(z_{k+1})] e^{\tau_\nu(z_n)} \left[e^{-\tau_\nu(z_{k+1})} - e^{-\tau_\nu(z_k)} \right] \tag{49}$$

The value of a_k can be determined by solution of the linear equation $\tau_\nu(s) = a_k s + b_k$ at the two endpoints of each interval as follows:

$$\tau_\nu(z_{k+1}) = a_k z_{k+1} + b_k \tag{50}$$

$$\tau_\nu(z_k) = a_k z_k + b_k \tag{51}$$

Subtracting the second equation from the first to eliminate b_k , we have

$$\begin{aligned}
\tau_\nu(z_{k+1}) - \tau_\nu(z_k) &= a_k z_{k+1} - a_k z_k \\
&= a_k (z_{k+1} - z_k) \tag{52}
\end{aligned}$$

So

$$a_k = \frac{\tau_\nu(z_{k+1}) - \tau_\nu(z_k)}{z_{k+1} - z_k} \tag{53}$$

which can be substituted in equations (48) and (49) to get

$$\begin{aligned}
I_{\nu}^{+}(z_n, 1) &= I_{\nu p}(T_w)e^{-\tau_{\nu}(z_n)} + \sum_{k=1}^{n-1} \frac{1}{2} \frac{z_{k+1} - z_k}{[\tau_{\nu}(z_{k+1}) - \tau_{\nu}(z_k)]} [j_{\nu}^e(z_k) + j_{\nu}^e(z_{k+1})] \\
&\quad \times e^{-\tau_{\nu}(z_n)} [e^{\tau_{\nu}(z_{k+1})} - e^{\tau_{\nu}(z_k)}]
\end{aligned} \tag{54}$$

$$\begin{aligned}
I_{\nu}^{-}(z_n, -1) &= -\sum_{k=n}^{k_{\max}-1} \frac{1}{2} \frac{z_{k+1} - z_k}{[\tau_{\nu}(z_{k+1}) - \tau_{\nu}(z_k)]} [j_{\nu}^e(z_k) + j_{\nu}^e(z_{k+1})] \\
&\quad \times e^{\tau_{\nu}(z_n)} [e^{-\tau_{\nu}(z_{k+1})} - e^{-\tau_{\nu}(z_k)}]
\end{aligned} \tag{55}$$

This piecewise linear treatment provides excellent results.

5.3.2. Special Case for Constant τ_{ν}

In some spectral and spatial regions, the optical variable may be essentially constant from one grid point to the next. When this situation occurs, the numerical integration developed above must be revisited. As seen in equations (54) and (55), division by zero occurs in this case. The integral in equation (45) can be more simply evaluated for constant τ_{ν} as

$$\begin{aligned}
\int_{z_k}^{z_{k+1}} e^{A_k x + B_k} dx &\approx \int_{z_k}^{z_{k+1}} e^{A_k z_k + B_k} dx \\
&= e^{A_k z_k + B_k} \int_{z_k}^{z_{k+1}} dx \\
&= e^{A_k z_k + B_k} (z_{k+1} - z_k)
\end{aligned} \tag{56}$$

After substituting this result in equations (43) and (44), we get

$$I_{\nu}^{+}(z_n, 1) = I_{\nu p}(T_w)e^{-\tau_{\nu}(z_n)} + \sum_{k=1}^{n-1} \frac{1}{2} [j_{\nu}^e(z_k) + j_{\nu}^e(z_{k+1})] e^{\tau_{\nu}(z_k) - \tau_{\nu}(z_n)} (z_{k+1} - z_k) \tag{57}$$

$$I_{\nu}^{-}(z_n, -1) = \sum_{k=n}^{k_{\max}-1} \frac{1}{2} [j_{\nu}^e(z_k) + j_{\nu}^e(z_{k+1})] e^{\tau_{\nu}(z_n) - \tau_{\nu}(z_k)} (z_{k+1} - z_k) \tag{58}$$

5.4. Flow-Field Coupling

The LAURA algorithm for solution of the Navier Stokes equations is summarized in reference 22. The divergence of the radiative flux can be treated as a source term in the two energy equations. In general, source terms are handled implicitly (ref. 29) in the LAURA algorithm. This treatment improves scheme stability and robustness. Radiation is sensitive to flow-field properties, so the added radiation source term should be treated implicitly. However, Park and Milos (ref. 30) have found this implicit treatment to be prohibitively expensive in computer time except for one-dimensional flows. Furthermore, the necessary terms for the Jacobian are nearly impossible to obtain in the current nonequilibrium treatment. Therefore, the radiation term is treated as an explicit (ref. 29) source term in the LAURA algorithm.

The convergence of the flow field in the LAURA code is characterized by transient waves in the gas properties. When the sensitive radiation calculation is performed on a flow field that still contains transients, the radiation term can change dramatically. This change can introduce additional fluctuations and lead to instability. In the present study, therefore, under-relaxation is applied to the explicit radiation source term. That is, the latest radiation solution is combined with the previous solution to compute an updated radiation term,

$$(\nabla \cdot \mathbf{q}_R)^{n'+1} = d_q(\nabla \cdot \mathbf{q}_R)^n + (1 - d_q)(\nabla \cdot \mathbf{q}_R)^{n+1} \quad (59)$$

The underrelaxation approach of equation (59) reduces the fluctuations due to coupling and increases the stability of the combined algorithm. A relaxation factor d_q of 0.5 has been used.

Because the flow properties change little in a single flow-field iteration and because flow-field transients should be allowed to decay, the radiative flux divergence term need not be updated with every flow field update. In fact, the total cost of the combined computation can be reduced several orders of magnitude by updating the radiation term a minimum number of times, as is successfully done in equilibrium shock-fitting methods. Updating it too rarely, however, can decrease the convergence rate, produce oscillatory nonconvergence, or destabilize the solution. For example, if the flow field changes dramatically between radiation term updates, a large change in the radiation will result and can introduce severe waves into the flow field. In addition, if flow structures change position significantly between updates of the radiation, the radiation term will be temporarily unaligned with the associated flow structure. Experience with cases characterized by a moderate degree of nonequilibrium suggests that updating the radiation calculation once every 500 flow-field updates provides reasonable convergence. For cases with more severe nonequilibrium in which coupling has a large effect on the standoff distance, more frequent updates are required (every 200 iterations). As a flow field approaches equilibrium, on the other hand, the current LAURA algorithm converges more slowly. For near-equilibrium cases, the radiation is updated only every 1000 to 5000 flow-field iterations. However, the optimal update interval may change if the LORAN code and a different CFD code are coupled.

Coupled solutions may be difficult to obtain when extreme gradients occur in the shock wave, as is the case for near-equilibrium flows. The computational mesh used in a flow-field calculation seldom provides adequate resolution in the shock region to produce smooth temperature profiles in such flows. This lack of resolution at the shock does not significantly degrade the flow-field solution. The radiation calculation is sensitive to temperature, however, so it can cause large changes in the profile of $\nabla \cdot \mathbf{q}_R$, which may lead to inaccurate results or even divergent solutions. Increasing the number of grid points can alleviate this problem but is not always practical because of storage limitations. Grid adaption, on the other hand, can improve the temperature profiles without increased storage. To provide this ability, a grid adaption algorithm has been added to the LAURA code. (See ref. 31.) This algorithm can be used to cluster grid points around a specified density or temperature in the shock.

The low-temperature (precursor) region ahead of the shock in a shock-capturing scheme also requires special treatment. The LORAN radiation model as currently implemented does not include accurate radiation properties at low temperatures. The precursor is generally assumed to have negligible effect on the converged flow field as it can absorb only a small fraction of the radiative energy passing through it. Recent results (ref. 32) confirm the validity of this approximation. Therefore, $\nabla \cdot \mathbf{q}_R$ is set to zero—the value appropriate for a nonparticipating medium—when the vibrational or translational temperature is below a certain minimum. This adjustment is done within the LAURA flow-field calculation every iteration. Even if accurate precursor (low-temperature) radiation properties are available, some logic is required at each iteration so that a decrease in shock standoff distance between radiation updates will not leave

a large radiation term in what is now the free stream. A temperature limit of 500 K provides good results for the cases so far examined.

As a practical matter, a converged flow-field solution should be obtained first with the LAURA code, then the radiation should be “turned on” to converge the coupled flow field. If the radiation is only a small perturbation to the flow field, this second convergence may require only a few additional LAURA iterations. If strong radiation effects are evident, then the perturbed flow field will require many additional iterations to converge. The optimal sequence for converging a coupled solution is not known; it must be learned by experience with the code.

6. Computational Optimization

Obtaining radiation predictions for complete flow fields or coupling radiation and flow-field solutions requires that the radiation calculations be carried out many times. To make this iteration practical and to minimize the cost, the radiation program should be optimized and the minimum set of calculations which will provide an accurate radiation prediction should be determined. The accuracy required will vary depending on the flow regime and body shape and on the intended use of the results. Therefore, an optimization study may be required for each project undertaken with the LORAN code. (An example is given in ref. 33.) Methods of achieving this optimization are discussed in sections 6.1.–6.3.

6.1. Radiation Calculation

Parametric studies can be conducted to determine the spectral resolution required for acceptable accuracy in the predicted radiation. The effects of the following variables should be studied: na , the number of points allowed in the atomic continuum spectrum; $nppl$; and nv , $crit$, and $crit2$, the several variables that control the generation of the spectrum for molecular band radiation. In addition, various sets of atomic lines can be inserted, from the fully detailed to a set of multiplet-averaged lines. The parameters and inputs should be chosen as appropriate for each study.

6.2. Excitation Calculation

The computing time required to obtain the nonequilibrium excited state populations is a significant fraction of the total for the LORAN code. The QSS algorithm used to perform this calculation was obtained from the NEQAIR program and is used as a “black box.” Improvements to this algorithm could significantly improve the computing efficiency of the radiation prediction. However, no changes have been made to date to take advantage of that savings.

6.3. Radiation Subgrid

Calculating radiative properties at every point on a flow-field grid is often wasteful. The absorption and emission coefficients change significantly only in regions with large gradients in temperature or species concentrations. Bolz (ref. 34) developed an algorithm to automatically select a subset of grid points for the radiation calculation. He defines a weighting function Z which can be adapted to the nonequilibrium situation as

$$\begin{aligned}
 Z_k = k + \sum_{i=1}^k & \left(W_N \frac{\bar{N}'_i}{\bar{N}'_{i,\max}} + W_{T_t} \frac{|T'_t|_i}{|T'_t|_{i,\max}} + W_{T_r} \frac{|T'_r|_i}{|T'_r|_{i,\max}} \right. \\
 & \left. + W_{T_v} \frac{|T'_v|_i}{|T'_v|_{i,\max}} + W_{T_e} \frac{|T'_e|_i}{|T'_e|_{i,\max}} + W_{\mathbf{qR}} \frac{|\mathbf{qR}'|_i}{|\mathbf{qR}'|_{i,\max}} \right) \quad (60)
 \end{aligned}$$

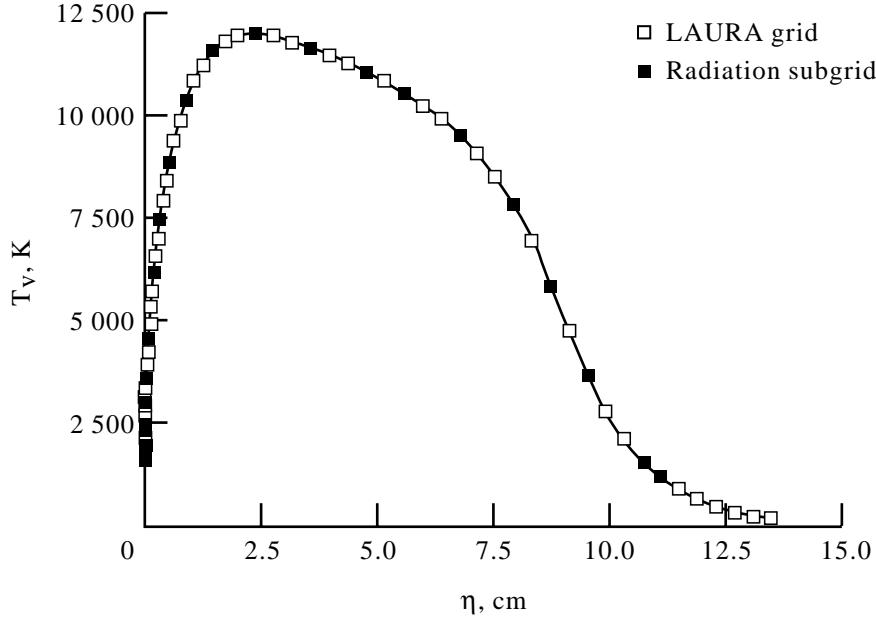


Figure 5. Example of radiation subgrid selection.

The prime in equation (60) denotes the partial derivative with respect to the normal to the wall. This quantity is evaluated at each normal grid point k in the flow field. If the vibrational temperatures of individual species are computed in the future, additional terms can be added to Z_k . The average derivative of the species number densities is

$$\overline{N}'_i = \frac{1}{n_s} \sum_{j=1}^{n_s} |N'_{i,j}| \quad (61)$$

for s chemical species. Radiation is then computed for a subset k_R of the flow-field grid points chosen at equal intervals of Z_k . An example of such a grid is given in figure 5. Although weighting factors W_i are included for each term in Z_k , the gradient in one variable should not necessarily be emphasized more than that of another. Therefore, these factors are all set equal to 1. In some applications, different values of the weighting factors may benefit the user. For optimal accuracy in a study, the size of the radiation subgrid k_R should also be varied. (See ref. 33 for an example.)

To further reduce the required computational time, every other normal line of the flow-field grid and every other plane in a three-dimensional solution might be skipped in the radiation calculation. The required radiation properties can be interpolated for the skipped normal lines. Although the subgrid algorithm could be applied in these directions also, the expected gradients are generally gentler and not as well suited to the method.

7. Using the Code

The code consists of 58 FORTRAN subroutines and 6 “include files” and has been run on Sun, Silicon Graphics, and Cray computers, all with UNIX operating systems. A “makefile” is available for compilation and loading. Double precision accuracy is required on the Sun and Silicon Graphics computers; on the Cray computer, single precision is adequate and much faster. Conversion to single precision requires removing implicit double precision statements everywhere, changing double precision declarations to real, and switching all intrinsic functions to a single precision form; otherwise, the user must employ an appropriate compiler option if

available. For a brief overview of the code, appendix C presents the code structure in the form of a subroutine calling tree.

The code is provided to potential users with sample input and output files to allow verification. Because these files are quite extensive, they are not included in this document. Examples of results obtained with the LORAN code can also be found in references 18, 26, 31, 33, and 35–38.

7.1. Include Files

The six include files set several important parameters for the code and have comments with descriptions of each variable. The following are the general functions of the include files:

<code>btask.zzzz</code>	storage for heat flux and flux divergence results
<code>geoa.zzzz</code>	storage of flow-field grid geometry
<code>parm1.zzzz</code>	parameters that set size of flow-field grid; must be changed for different grid sizes
<code>parm2.zzzz</code>	parameters that set number of species; no change if air
<code>parm4.zzzz</code>	grid singularity flag
<code>parr.zzzz</code>	parameters that set radiation subgrid size and control optimized radiation spectrum; change for different grid sizes and spectral resolution

7.2. Input Files

Two input files are required:

<code>neq.in</code>	contains excitation and radiation data adapted from NEQAIR input files
<code>radneq.in</code>	contains control and line data adapted from RAD/EQUIL input

These files are opened in the code so need only be present in the directory where the code is being run. An input guide is included in appendix D. Except for a few variables near the beginning of file `radneq.in`, most of these variables will not be changed by the user. The description of the variables is provided to aid in understanding the code and for adding to or updating the excitation and radiation properties.

Although the input has provision for 25 species, with 22 ordered as in the RAD/EQUIL code and with 3 spares, the LORAN code does not yet contain radiative properties for all these species. Some properties are available for N, O, C, N⁺, O⁺, C⁺, e⁻, N₂, O₂, NO, C₂, CO, CN, and N₂⁺. For N, O, and C, bound-free and line radiation is computed. For N⁺, O⁺, and C⁺, free-free radiation is considered. The following molecular radiative transitions are included: N₂⁺(1⁻); N₂(1⁺); N₂(2⁺); N₂ Birge-Hopfield; NO β, NO γ, and O₂ Schumann-Runge; CN violet; CN red; CO(4⁺); and C₂ Swings bands. As more properties become available, they will be added to the LORAN input set.

Flow-field condition input is also required through some interface. In the stand-alone LORAN code, these data reside in the file `restart.dat`, which is also opened in the code.

7.3. Output Files

The following output files may be produced, depending on the control flags set:

standard output	name may be set by user; contains FORTRAN errors and warnings; echoes parameter values used; summarizes spectrum and flux calculation
-----------------	---

<code>flow.out</code>	single-zone I-ordered Tecplot ² computer file that contains normal coordinate and flow-field properties along stagnation grid line with 4 temperatures and 11 species number densities (for air)
<code>fluxdiv.out</code>	single-zone IJ-ordered Tecplot file that contains grid coordinates and divergence of radiative flux for each normal grid line
<code>qr.out</code>	multizone I-ordered Tecplot file that contains normal grid coordinate and positive and negative intensity/flux (I_ν^+ and I_ν^- or q_ν^+ and q_ν^-) for each normal grid line (one zone per grid line); uses block format
<code>rademis.out</code>	single-zone IJ-ordered Tecplot file that contains grid coordinates and radiative emission at each point in radiation subgrid; includes atomic continuum, molecular, atomic line, visible, and infrared-only atomic line emission
<code>radneq.out</code>	summary of data input and radiation calculation; gives total emission results and reports irregularities in calculation
<code>walrad.out</code>	single-zone I-ordered Tecplot file that contains path length coordinate, upper limit of spectral range, and wall radiative intensity/flux at each surface grid point
<code>wsp.out</code>	multizone I-ordered Tecplot file that contains spectral output: frequency points, spectral intensity/flux, and running integral of intensity/flux for each normal grid line (one zone per grid line)

Tecplot files are the input files for the Tecplot plotting program. (See ref. 39.) A description of their format is given in appendix E.

8. Conclusions

A new method for computing radiative heating in thermochemical nonequilibrium flow fields has been developed. This method takes advantage of a priori knowledge of the radiation spectrum to generate an optimized spectral array for radiation calculations. Computational efficiency is further enhanced by the assumption of smeared molecular bands. The theoretical basis and practical application of the method have been summarized here.

NASA Langley Research Center
Hampton, VA 23681-0001
May 23, 1994

²Tecplot: trademark of Amtec Engineering, Inc., Bellevue, WA, 98009-3633.

Appendix A

Gaussian Units

For the reader's convenience, the Gaussian system of units is redefined here.

c	speed of light in vacuum, 2.9979×10^{10} cm/sec
e	electron charge, 4.80286×10^{-10} statcoulomb
h	Planck's constant, 6.6262×10^{-27} erg-sec
k	Boltzmann's constant, 1.3807×10^{-16} erg/K
m_e	electron mass, 9.1095×10^{-28} g

The following relations hold among several of these quantities:

The Bohr radius a_0 is given by

$$\begin{aligned} a_0 &= \frac{h^2}{4\pi^2 m_e e^2} \\ &= 0.52918 \times 10^{-8} \text{ cm} \end{aligned}$$

The fine structure constant α , a dimensionless quantity, is

$$\begin{aligned} \alpha &= \frac{2\pi e^2}{hc} \\ &= 7.292 \times 10^{-3} \end{aligned}$$

Appendix B

Molecular Radiation Model

Smearred Band Derivation

In the discussion that follows, Zeldovich-Raizer refers to reference 9; Herzberg refers to reference 13. The energy differentials for the molecular transitions are established first. The expressions given below for the energy levels are to some extent based on curve fits. In most cases, improvements are possible.

For electronic transitions, the energy levels are given by E_e , the electron energy of a particular energy level measured from the ground state. For vibrational transitions, the energy levels are obtained from the fourth-order expression given by Herzberg,

$$E_v = hc \left[\omega_e \left(v + \frac{1}{2} \right) - \omega_e x_e \left(v + \frac{1}{2} \right)^2 + \omega_e y_e \left(v + \frac{1}{2} \right)^3 + \omega_e z_e \left(v + \frac{1}{2} \right)^4 \right] \quad (\text{B1})$$

which includes a correction for the anharmonicity of the vibrational energy potential. The vibrational levels range from the zero-point energy at $v = 0$ to some maximum v determined by the dissociation of the molecule. The coefficients in the above expression are spectroscopic constants and are available from several sources. The values used in the LORAN code are those collected by Park for the NEQAIR code. The energy levels for the rotational transitions, including a correction for nonrigid oscillators, are

$$E_r = hc \left[B_v J(J+1) - D_v J^2(J+1)^2 \right] \quad (\text{B2})$$

where the spectroscopic constant B_v has been corrected for rotational effects as

$$B_v = B_e - \alpha_e \left(v + \frac{1}{2} \right) \quad (\text{B3})$$

and the second rotational spectroscopic constant D_v is

$$\begin{aligned} D_v &= D_e + \beta_e \left(v + \frac{1}{2} \right) \\ &\approx D_e \\ &= \frac{4B_e^3}{\omega_e^2} \end{aligned} \quad (\text{B4})$$

These levels range from zero energy at $J = 0$ to some maximum J , again determined by dissociation of the molecule for each vibrational level. The spectroscopic constants for rotational energy states are also those collected by Park.

The complete molecular energy level is

$$E_{\text{tot}} = E_e + E_v + E_r \quad (\text{B5})$$

where the individual energy contributions are given by equations (B1) and (B2) above. Designating the upper level by the superscript u and the lower level by l , the wave number (inverse wavelength) of a particular transition is

$$\frac{1}{\lambda} = \frac{E_{\text{tot}}^u - E_{\text{tot}}^l}{hc} \quad (\text{B6})$$

For convenience in manipulating these expressions, one special wave number is defined, the wave number with zero rotational quantum number and arbitrary vibrational quantum numbers. Thus,

$$\frac{1}{\lambda_{v^u v^l}} = \frac{E_e^u - E_e^l}{hc} + \frac{E_v^u - E_v^l}{hc} \quad (\text{B7})$$

The formidable expression for the wave number of an individual transition is simplified by the selection rules for rotation. (See refs. 9 and 13.) A detailed discussion of these selection rules and of the designation of molecular states is outside the scope of the present work. Nevertheless, these rules allow the development of three specific wave numbers for the transitions $\Delta J = -1$, 0, and 1, which are denoted P, Q, and R, respectively. Therefore,

$$\begin{aligned} \frac{1}{\lambda_P} = & \frac{1}{\lambda_{v^u v^l}} + (J^l)^4 (D_e^l - D_e^u) + (J^l)^3 (2D_e^l + 2D_e^u) \\ & + (J^l)^2 (D_e^l - B_v^l - D_e^u + B_v^u) + J^l (-B_v^u - B_v^l) \end{aligned} \quad (\text{B8})$$

$$\begin{aligned} \frac{1}{\lambda_Q} = & \frac{1}{\lambda_{v^u v^l}} + (J^l)^4 (D_e^l - D_e^u) + (J^l)^3 (2D_e^l - 2D_e^u) \\ & + (J^l)^2 (D_e^l - B_v^l - D_e^u + B_v^u) + J^l (B_v^u - B_v^l) \end{aligned} \quad (\text{B9})$$

$$\begin{aligned} \frac{1}{\lambda_R} = & \frac{1}{\lambda_{v^u v^l}} + (J^l)^4 (D_e^l - D_e^u) + (J^l)^3 (2D_e^l - 6D_e^u) \\ & + (J^l)^2 (D_e^l - B_v^l - 13D_e^u + B_v^u) + J^l (3B_v^u - 12D_e^u - B_v^l) + 2B_v^u - 4D_e^u \end{aligned} \quad (\text{B10})$$

After the molecular band spectra are thus determined, the probability of a transition between levels must be evaluated to obtain an expression for the absorption coefficient. This probability is obtained from a quantum mechanical analysis. The resulting expression for the transition probability is given in Zeldovich-Raizer:

$$\begin{aligned} A_{ul} = & A_{Av^l J^l}^{Bv^u J^u} \\ = & \frac{64\pi^4}{3g_B h c^3} \left(\nu_{Bv^u J^u, Av^l J^l} \right)^3 D_{elBA}^2 q_{v^u v^l} p_{J^u J^l} \end{aligned} \quad (\text{B11})$$

where the upper state degeneracy g_B has been added to the denominator to account for degenerate states. (See ref. 13, p. 21.) Also, $q_{v^u v^l}$ is the Franck-Condon factor for the probability of a vibrational transition, $p_{J^u J^l}$ is the probability of a rotational transition, and D_{elBA}^2 is the square of the matrix element (*sre2*, used by Park in the NEQAIR code, is the nondimensional value, which is divided by $(a_0 e)^2$, the squared product of the Bohr radius and the charge of an electron) arising from the wave function in the quantum mechanical analysis. The Einstein coefficient for spontaneous emission is A and super- and subscripts A and B denote the lower and upper electronic states of the molecule, respectively. Using the principle of detailed balancing leads to the well-known relationship between the Einstein coefficients for emission and absorption (i.e., refs. 27 or 9),

$$B_{lu} = \frac{c^2}{8\pi h \nu_{ul}^3} \frac{g_u}{g_l} A_{ul} \quad (\text{B12})$$

If this relationship is expressed for energy states rather than energy levels, the degeneracies g_u and g_l are identically one, by definition. As a practical matter, the use of energy levels, which may be degenerate, is preferred because it reduces the bookkeeping required.

The absorption coefficient κ_{lu} is related to the Einstein coefficient for absorption B_{lu} (ref. 40) by

$$\kappa_{lu} = n_l B_{lu} h \nu_{lu} \quad (\text{B13})$$

Substituting equations (B11) and (B12) in this last expression yields the desired expression for the spectral absorption coefficient,

$$\kappa_{\nu_{Av^l J^l, Bv^u J^u}} = \frac{g_{Bv^u J^u}}{g_{Av^l J^l}} \frac{8\pi^3}{3g_B h c} N_{Av^l J^l} (\nu_{Av^l J^l, Bv^u J^u}) D_{elBA}^2 q_{v^u v^l} p_{J^u J^l} F(\nu) \quad (\text{B14})$$

where $F(\nu)$ is a normalized line shape. This expression must be evaluated for each A , B , v^u , v^l , J^u , and J^l to obtain the complete absorption spectrum of a molecular species. The smeared band model averages out the rotational line structure by summing equation (B14) over J^u and introducing an average frequency $\bar{\nu}_{Bv^u, Av^l}$ for the rotational lines. The result is

$$\kappa_{\nu_{Av^l J^l, Bv^u}} = \frac{8\pi^3}{3h c} \frac{1}{g_A} N_{Av^l J^l} D_{elBA}^2 q_{v^u v^l} F(\nu) \bar{\nu}_{Bv^u, Av^l} \quad (\text{B15})$$

where use has been made of the relation $\sum_{J^u}^{\infty} p_{J^u J^l} = 1$, which expresses the fact that all transitions occur between two levels of the molecule. The degeneracy has been expanded into its components,

$$g_{Av^l J^l} = g_A g_{v^l} g_J \quad (\text{B16})$$

where

$$g_{v^l} = 1 \quad (\text{B17})$$

because no degenerate vibrational levels exist and

$$g_J = 2J + 1 \quad (\text{B18})$$

For most rotational lines, $J \gg 1$ and the ratio of rotational degeneracies in equation (B14) is approximately equal to 1. This approximation has been used even for transitions with low values of J . The error introduced in a single transition with a low rotational quantum number can be as much as 300 percent; however, only a few transitions have low J , so that the effect on the overall absorption coefficient is small. The error incurred by introducing the average frequency $\bar{\nu}_{Bv^u, Av^l}$ for all rotational lines in the band $v^l - v^u$ is minimal, ≈ 1 to 7 percent.

To obtain the complete absorption coefficient, equation (B15) is now summed over the final vibrational level v^u . This summation yields

$$\kappa_{\nu_{Av^l J^l, B}} = \frac{8\pi^3}{3h c} \frac{1}{g_A} N_{Av^l J^l} D_{elBA}^2 F(\nu) \sum_{v^u}^{\infty} q_{v^u v^l} \bar{\nu}_{Bv^u, Av^l} \quad (\text{B19})$$

Here, the frequency remains inside the summation and is not averaged, as the variation can be large.

The mean value theorem is then used to define an average absorption coefficient for a line by integrating over one line width for

$$\int_{\text{line}} \kappa_{\nu_{Av^l J^l, B}} d\nu = \frac{8\pi^3}{3h c} \frac{1}{g_A} N_{Av^l J^l} D_{elBA}^2 \sum_{v^u}^{\infty} q_{v^u v^l} \bar{\nu}_{Bv^u, Av^l} = \bar{\kappa}_{\nu_{Av^l J^l, B}} \Delta\nu \quad (\text{B20})$$

where $\Delta\nu$ is the line width.

Equation (B20) is then solved for $\bar{\kappa}_\nu$ and summed over the initial rotational and vibrational levels to obtain

$$\bar{\kappa}_{\nu AB} = \frac{8\pi^3}{3hc} \frac{1}{g_A} D_{elBA}^2 \sum_{v^l} \sum_{v^u} q_{v^u, v^l} \bar{\nu}_{Bv^u, Av^l} \sum_{J^l} \frac{N_{Av^l J^l}}{\Delta\nu} \quad (\text{B21})$$

where the sum term is zero for any transition which does not absorb radiation in the frequency interval considered.

Equation (B21) is the complete formula for the smeared band absorption coefficient for a molecular species. In this form it contains two approximations: an average frequency for the rotational lines in a vibrational band and the averaging over a single line. To use this expression in a radiation model, the various parts must now be amplified in terms of known quantities.

In nonequilibrium conditions, the number density in a particular energy level is given by the following expression, where the existence of rotational and vibrational temperatures and the separability of the rotational and vibrational energy modes have been assumed:

$$N_{Av^l J^l} = N_A \frac{\exp(-E_{v^l}/kT_v) g_{J^l} \exp(-E_{J^l}/kT_r)}{Q_v(T_v) Q_r(T_r)} \quad (\text{B22})$$

where Q_v and Q_r are the vibrational and rotational partition functions, respectively. The population of the electronic energy level N_A must be obtained from some nonequilibrium excitation calculation. In the present work, Park's QSS method (ref. 14) has been used. The partition functions are obtained from their definition

$$Q_i(T_i) = \sum_{i=0}^{\infty} \exp(-E_i/kT_i) \quad (\text{B23})$$

In practice, the upper limit of this summation is imposed either by predissociation in the rotational case or by numerical limits arising from inaccuracies in the higher order coefficients of equation (B1) for the vibrational case. (The rotational case is discussed in a separate section below.) For the vibrational case, the sum may be terminated when the contribution of the next term is less than some threshold percentage of the partition function. The size of each term must also be monitored to detect the onset of significant inaccuracies in equation (B1); these inaccuracies occur at a high enough vibrational quantum number that the sum for the partition function can be truncated at that point.

The next term to be examined in equation (B21) is $\Delta\nu$, which introduces another approximation of the smeared band model. The line width $\Delta\nu$ is assumed to be approximately equal to an average line spacing. To evaluate the line spacing, consider the three expressions for the line centers, equations (B8)–(B10). If the terms D_e are neglected compared with the terms B_v (they are much smaller), the equations reduce to

$$\frac{1}{\lambda_P} = \frac{1}{\lambda_{v^u v^l}} + (J^l)^2 (B_v^u - B_v^l) + J^l (-B_v^u - B_v^l) \quad (\text{B24})$$

$$\frac{1}{\lambda_Q} = \frac{1}{\lambda_{v^u v^l}} + (J^l)^2 (B_v^u - B_v^l) + J^l (B_v^u - B_v^l) \quad (\text{B25})$$

$$\frac{1}{\lambda_R} = \frac{1}{\lambda_{v^u v^l}} + (J^l)^2 (B_v^u - B_v^l) + J^l (3B_v^u - B_v^l) + 2B_v^u \quad (\text{B26})$$

For a line with $J^l \gg 1$, which is the case for most lines, these three expressions collapse into the single form

$$\begin{aligned} \frac{1}{\lambda} &= \frac{\nu}{c} \\ &\approx \frac{1}{\lambda_{v^u v^l}} + (J^l)^2 (B_v^u - B_v^l) \end{aligned} \quad (\text{B27})$$

Solving for ν and taking the derivative with respect to J (remembering that $\Delta J = 1$ for adjacent lines) gives

$$\Delta\nu = 2cJ^l |B_{v^u} - B_{v^l}| \quad (\text{B28})$$

where the absolute value is taken to ensure that the average spacing is positive. Equation (B27) also yields an approximate expression for J^l in terms of the wavelength or wave number

$$(J^l)^2 \approx \left(\frac{1}{\lambda} - \frac{1}{\lambda_{v^u v^l}} \right) \frac{1}{B_{v^u} - B_{v^l}} \quad (\text{B29})$$

Because $(J^l)^2 > 0$, the right side of this equation must also be positive. This situation implies for $B_{v^u} > B_{v^l}$ that $\lambda_{v^u v^l} > \lambda$ and for $B_{v^u} < B_{v^l}$ that $\lambda_{v^u v^l} < \lambda$. These requirements are the mathematical statements of the fact that each vibrational band absorbs in only a portion of the spectrum. In an evaluation of the absorption coefficient for a particular band, the wavelength or frequency considered must be checked for the above conditions to avoid superfluous contributions.

The rotational energy levels in equation (B2) contain the assumption that $J^l \gg 1$. This assumption allows the replacements $J^l + 1 \approx J^l$ and $2J^l + 1 \approx 2J^l$. Equation (B29) can then be substituted in equation (B2) with the result

$$\begin{aligned} E_r \approx hc \left\{ \left[B_e^l - \alpha_e^l \left(v^l + \frac{1}{2} \right) \right] \left(\frac{1}{\lambda} - \frac{1}{\lambda_{v^u v^l}} \right) \frac{1}{B_{v^u} - B_{v^l}} \right. \\ \left. - \frac{4(B_e^l)^3}{(\omega_e^l)^2} \left(\frac{1}{\lambda} - \frac{1}{\lambda_{v^u v^l}} \right)^2 \frac{1}{(B_{v^u} - B_{v^l})^2} \right\} \end{aligned} \quad (\text{B30})$$

This expression can then be substituted in the rotational exponent in equation (B22). It constitutes the final approximation of the smeared band model.

The last term to evaluate in equation (B21) is the averaged frequency $\bar{\nu}_{B_{v^u}, A_{v^l}}$. This term must be evaluated separately for so-called Σ and non- Σ transitions according to the rotational selection rules mentioned above. For a given vibrational transition, equations (B8)–(B10) describe the line centers of each rotational transition (eq. (B9) is not allowed for Σ transitions). Because the 0-0 rotational transition is always forbidden, $\bar{\nu}_{B_{v^u}, A_{v^l}}$ can be evaluated as follows:

$$\begin{aligned} \bar{\nu}_{B_{v^u}, A_{v^l}} &= \overline{\left(\frac{c}{\lambda} \right)}_{B_{v^u}, A_{v^l}} \\ &= \frac{c}{3J_{\max}^l + 1} \left[\sum_{J^l=1}^{J_{\max}^l} \left(\frac{1}{\lambda_P} + \frac{1}{\lambda_Q} + \frac{1}{\lambda_R} \right) + \frac{1}{\lambda_R|_{J^l=0}} \right] \end{aligned} \quad (\text{B31})$$

$$\begin{aligned}
\bar{\nu}_{Bv^u,Av^l} &= \overline{\left(\frac{c}{\lambda}\right)}_{Bv^u,Av^l} \\
&= \frac{c}{2J_{\max}^l + 1} \left[\sum_{J^l=1}^{J_{\max}^l} \left(\frac{1}{\lambda_P} + \frac{1}{\lambda_R} \right) + \frac{1}{\lambda_R|_{J^l=0}} \right]
\end{aligned} \tag{B32}$$

where equation (B31) is for non- Σ transitions and equation (B32) is for Σ transitions.

Substituting equations (B8)–(B10) in equations (B31) and (B32) and collecting terms result in the following expressions for the averaged frequency:

$$\begin{aligned}
\bar{\nu}_{Bv^u,Av^l} &= \frac{c}{\lambda_{v^u v^l}} + \frac{c(J_{\max}^l + 1)}{3J_{\max}^l + 1} (2B_v^u - 4D_e^u) + \frac{c}{3J_{\max}^l + 1} \\
&\times \left\{ (3D_e^l - 3D_e^u) (J_{\max}^l + 1) (2J_{\max}^l + 1) \left[3(J_{\max}^l)^2 + 3J_{\max}^l + 1 \right] \frac{J_{\max}^l}{30} \right. \\
&+ (6D_e^l - 6D_e^u) \frac{(J_{\max}^l)^2 (J_{\max}^l + 1)^2}{4} + (3B_v^u - 3B_v^l - 15D_e^u + 3D_e^l) \\
&\times \left. \frac{J_{\max}^l (J_{\max}^l + 1) (2J_{\max}^l + 1)}{6} + (3B_v^u - 3B_v^l - 12D_e^u) \frac{J_{\max}^l (J_{\max}^l + 1)}{2} \right\} \tag{B33}
\end{aligned}$$

$$\begin{aligned}
\bar{\nu}_{Bv^u,Av^l} &= \frac{c}{\lambda_{v^u v^l}} + \frac{c(J_{\max}^l + 1)}{2J_{\max}^l + 1} (2B_v^u - 4D_e^u) + \frac{c}{2J_{\max}^l + 1} \\
&\times \left\{ (2D_e^l - 2D_e^u) (J_{\max}^l + 1) (2J_{\max}^l + 1) \left[3(J_{\max}^l)^2 + 3J_{\max}^l + 1 \right] \frac{J_{\max}^l}{30} \right. \\
&+ (4D_e^l - 4D_e^u) \frac{(J_{\max}^l)^2 (J_{\max}^l + 1)^2}{4} + (2B_v^u - 2B_v^l - 14D_e^u + 2D_e^l) \\
&\times \left. \frac{J_{\max}^l (J_{\max}^l + 1) (2J_{\max}^l + 1)}{6} + (2B_v^u - 2B_v^l - 12D_e^u) \frac{J_{\max}^l (J_{\max}^l + 1)}{2} \right\} \tag{B34}
\end{aligned}$$

where again the first form is for non- Σ transitions and the second is for Σ transitions. These equations could be implemented as is; however, the result is simpler and still accurate if the terms D_e are neglected compared with the terms B_v . The result is

$$\bar{\nu}_{Bv^u,Av^l} = c \left[\frac{1}{\lambda_{v^u v^l}} + \frac{2B_v^u (J_{\max}^l + 1)}{3J_{\max}^l + 1} + \frac{3(B_v^u - B_v^l)}{3J_{\max}^l + 1} J_{\max}^l (J_{\max}^l + 1) (J_{\max}^l + 2) \right] \tag{B35}$$

$$\bar{\nu}_{Bv^u,Av^l} = c \left[\frac{1}{\lambda_{v^u v^l}} + \frac{2B_v^u (J_{\max}^l + 1)}{2J_{\max}^l + 1} + \frac{2(B_v^u - B_v^l)}{2J_{\max}^l + 1} J_{\max}^l (J_{\max}^l + 1) \frac{(J_{\max}^l + 2)}{3} \right] \tag{B36}$$

These equations for non- Σ and Σ transitions can then be substituted in equation (B21) and the averaged spectral absorption coefficient can be calculated.

The final result for the smeared band molecular absorption coefficient is

$$\begin{aligned}
\bar{\kappa}_{\nu_{AB}} &= \frac{8\pi^3}{3hc} \frac{1}{g_A} D_{\text{el}BA}^2 \sum_{v^l} \sum_{v^u} q_{v^u v^l} \bar{\nu}_{Bv^u, Av^l} \\
&\times \sum_{J^l} N_A \left[\frac{\exp(-E_{v^l}/kT_v)}{Q_v(T_v)} \frac{2J^l + 1}{2cJ^l |B_{v^u} - B_{v^l}| Q_r(T_r)} \right. \\
&\times \exp \left(-hc \left\{ \left[B_e^l - \alpha_e^l \left(v^l + \frac{1}{2} \right) \right] \left(\frac{1}{\lambda} - \frac{1}{\lambda_{v^u v^l}} \right) \frac{1}{B_{v^u} - B_{v^l}} \right. \right. \\
&\left. \left. - \frac{4(B_e^l)^3}{(\omega_e^l)^2} \left(\frac{1}{\lambda} - \frac{1}{\lambda_{v^u v^l}} \right)^2 \frac{1}{(B_{v^u} - B_{v^l})^2} \right\} / kT_r \right) \left. \right] \quad (\text{B37})
\end{aligned}$$

where $\bar{\nu}$ is given by equation (B35) for non- Σ transitions and by equation (B36) for Σ transitions, and the vibrational energy E_{v^l} is evaluated from equation (B1) with the appropriate values for the lower energy level. To be consistent, the approximation $2J^l + 1 \approx 2J^l$ is used to reduce the fraction inside the summation over J^l .

Alternatively, the mean value theorem can be applied in equation (B14) to obtain an average absorption coefficient for a single rotational line. The same summations and averaging as above can then be performed. The only difference from the result in equation (B37) is that the averaged frequency $\bar{\nu}_{Bv^u, Av^l}$ is replaced by $\nu_{Av^l J^l, Bv^u J^l}$, which is essentially the speed of light times the wave number λ^{-1} appearing in the exponential term above. This substitution eliminates the need for the calculation of $\bar{\nu}_{Bv^u, Av^l}$. The approximations required to obtain this result are that

$$\begin{aligned}
\nu_{Av^l J^l, Bv^u J^l} &\approx \nu_{Av^l J^l, Bv^u J^l + 1} \\
&\approx \nu_{Av^l J^l, Bv^u J^l - 1} \quad (\text{B38})
\end{aligned}$$

which must be true for the closely spaced rotational levels, and that

$$\frac{2J^u + 1}{2J^l + 1} \approx 1 \quad (\text{B39})$$

for $J^u = J^l$, $J^u = J^l - 1$, and $J^u = J^l + 1$. As discussed above, this approximation will be true except for a few low values of J and is acceptable. In general, it will introduce less errors than would the calculation of $\bar{\nu}_{Bv^u, Av^l}$. This alternate smeared band development is used in the LORAN code for both emission and absorption, although the coding for both has been retained. The smeared band absorption coefficient is then

$$\begin{aligned}
\bar{\kappa}_{\nu_{AB}} &= \frac{8\pi^3}{3hc} \frac{1}{g_A} D_{\text{el}BA}^2 \sum_{v^l} \sum_{v^u} \frac{q_{v^u v^l}}{\lambda} \sum_{J^l} \frac{N_A}{Q_v(T_v)} \left[\frac{\exp(-E_{v^l}/kT_v)}{|B_{v^u} - B_{v^l}| Q_r(T_r)} \right. \\
&\times \exp \left(-hc \left\{ \left[B_e^l - \alpha_e^l \left(v^l + \frac{1}{2} \right) \right] \left(\frac{1}{\lambda} - \frac{1}{\lambda_{v^u v^l}} \right) \frac{1}{B_{v^u} - B_{v^l}} \right. \right. \\
&\left. \left. - \frac{4(B_e^l)^3}{(\omega_e^l)^2} \left(\frac{1}{\lambda} - \frac{1}{\lambda_{v^u v^l}} \right)^2 \frac{1}{(B_{v^u} - B_{v^l})^2} \right\} / kT_r \right) \left. \right] \quad (\text{B40})
\end{aligned}$$

A smeared band expression can be developed for the molecular emission coefficient by a process parallel to that for absorption. The total emission in a rotational line J_{ul}^e is obtained from the Einstein coefficient for spontaneous emission:

$$J_{ul}^e = N_u A_{ul} h \nu_{ul} \quad (\text{B41})$$

The emission intensity at a particular frequency is obtained by dividing by the solid angle and introducing $F(\nu)$. Thus,

$$j_{\nu_{ul}}^e = \frac{N_u A_{ul} h \nu_{ul}}{4\pi} F(\nu) \quad (\text{B42})$$

Substituting equation (B11) for the Einstein coefficient yields

$$j_{\nu_{ul}}^e = N_u \frac{16\pi^3}{3g_B c^2} \nu_{ul}^4 D_{elBA}^2 q_{v^u v^l} p_{J^u J^l} F(\nu) \quad (\text{B43})$$

To obtain the smeared band result, this expression must first be summed over J^l and the average frequency $\bar{\nu}_{Bv^u, Av^l}$ introduced. Using the summation rule for $p_{J^u J^l}$ gives

$$j_{\nu_{Av^l, Bv^u J^u}}^e = N_{Bv^u J^u} \frac{16\pi^3}{3g_B c^2} (\bar{\nu}_{Bv^u, Av^l})^4 D_{elBA}^2 q_{v^u v^l} F(\nu) \quad (\text{B44})$$

In parallel to the development for absorption, the sum over v^l is now performed. Thus,

$$j_{\nu_{A, Bv^u J^u}}^e = N_{Bv^u J^u} \frac{16\pi^3}{3g_B c^2} D_{elBA}^2 F(\nu) \sum_{v^l} q_{v^u v^l} (\bar{\nu}_{Bv^u, Av^l})^4 \quad (\text{B45})$$

where again the frequency remains inside this summation for accuracy. The average emission coefficient for a single rotational line is now obtained using the mean value theorem,

$$\begin{aligned} \int_{\text{line}} j_{\nu_{A, Bv^u J^u}}^e d\nu &= \frac{16\pi^3}{3g_B c^2} D_{elBA}^2 N_{Bv^u J^u} \sum_{v^l} q_{v^u v^l} (\bar{\nu}_{Bv^u, Av^l})^4 \\ &= \bar{j}_{\nu_{A, Bv^u J^u}}^e \Delta\nu \end{aligned} \quad (\text{B46})$$

This equation can now be solved for the rotationally averaged emission coefficient. The complete smeared band emission coefficient is then obtained by summations over the final rotational and vibrational levels J^u and v^u . The result is

$$\bar{j}_{\nu_{AB}}^e = \frac{16\pi^3}{3g_B c^2} D_{elBA}^2 \sum_{v^u} \sum_{v^l} q_{v^u v^l} (\bar{\nu}_{Bv^u, Av^l})^4 \sum_{J^u} \frac{N_{Bv^u J^u}}{\Delta\nu} \quad (\text{B47})$$

As in the case for absorption, the infinite sums are truncated by dissociation.

The average frequency $\bar{\nu}_{Bv^u, Av^l}$ in equation (B47) is the same as that for absorption and is given by equations (B35) and (B36) for non- Σ and Σ transitions, respectively. The average line spacing is also the same and is given by the expression in equation (B28) with the rotational quantum number expressed in terms of the wave number according to equation (B29). The final term in the emission coefficient, the nonequilibrium upper level population, is found from the expression

$$N_{Bv^u J^u} = N_B \frac{\exp(-E_{v^u}/kT_v) g_{J^u} \exp(-E_{J^u}/kT_r)}{Q_v(T_v) Q_r(T_r)} \quad (\text{B48})$$

where the vibrational and rotational energies are given as a function of wave number by equations (B1) and (B30), evaluated for the upper energy level, and the electronic level population N_B is obtained from the QSS method. The evaluation of the partition functions was discussed in the section on absorption.

Substituting all these expressions in the emission coefficient of equation (B47) yields the smeared band result

$$\begin{aligned}
\bar{j}_{\nu AB}^e &= \frac{16\pi^3}{3g_B c^2} D_{elBA}^2 \sum_{v^u}^{\infty} \sum_{v^l}^{\infty} q_{v^u v^l} \left(\bar{\nu}_{Bv^u, Av^l} \right)^4 \\
&\times \sum_{J^u}^{\infty} N_B \left[\frac{\exp(-E_{v^u}/kT_v)}{Q_v(T_v)} \frac{2J^u + 1}{2cJ^u |B_{v^u} - B_{v^l}| Q_r(T_r)} \right. \\
&\times \exp \left(-hc \left\{ \left[B_e^u - \alpha_e^u \left(v^u + \frac{1}{2} \right) \right] \left(\frac{1}{\lambda} - \frac{1}{\lambda_{v^u v^l}} \right) \frac{1}{B_{v^u} - B_{v^l}} \right. \right. \\
&\left. \left. - \frac{4(B_e^u)^3}{(\omega_e^u)^2} \left(\frac{1}{\lambda} - \frac{1}{\lambda_{v^u v^l}} \right)^2 \frac{1}{(B_{v^u} - B_{v^l})^2} \right\} / kT_r \right) \right] \quad (B49)
\end{aligned}$$

Again, the approximation $2J^u + 1 \approx 2J^u$ is used inside the summation over J^u for consistency with the level of accuracy of the result.

As mentioned above, an alternate development is possible in which the mean value theorem is applied to equation (B43). This alternate model in which $\bar{\nu}_{Bv^u, Av^l}$ is replaced by $\nu_{Av^l J^l, Bv^u J^l}$ is the one implemented in the LORAN code, although coding for both has been retained. The smeared band emission is then calculated from

$$\begin{aligned}
\bar{j}_{\nu AB}^e &= \frac{16\pi^3}{3g_B c^2} D_{elBA}^2 \sum_{v^u}^{\infty} \sum_{v^l}^{\infty} q_{v^u v^l} \frac{c^3}{\lambda^4} \sum_{J^u}^{\infty} \frac{N_B}{Q_v(T_v)} \left[\frac{\exp(-E_{v^u}/kT_v)}{|B_{v^u} - B_{v^l}| Q_r(T_r)} \right. \\
&\times \exp \left(-hc \left\{ \left[B_e^u - \alpha_e^u \left(v^u + \frac{1}{2} \right) \right] \left(\frac{1}{\lambda} - \frac{1}{\lambda_{v^u v^l}} \right) \frac{1}{B_{v^u} - B_{v^l}} \right. \right. \\
&\left. \left. - \frac{4(B_e^u)^3}{(\omega_e^u)^2} \left(\frac{1}{\lambda} - \frac{1}{\lambda_{v^u v^l}} \right)^2 \frac{1}{(B_{v^u} - B_{v^l})^2} \right\} / kT_r \right) \right] \quad (B50)
\end{aligned}$$

Maximum Rotational Quantum Number

The maximum rotational quantum number J_{\max} can be determined to varying levels of approximation. The first-order calculation would predict the maximum when the energy of a level exceeds the dissociation energy of the species. As discussed in Herzberg (ref. 13), however, predissociation may occur due to the shape of the energy potential curve. Whiting, Arnold, and Lyle (ref. 41) developed a computer code based on this fact to predict the maximum rotational quantum number. The method was later refined by E. E. Whiting, Eloret Institute, Sunnyvale, California, in a private communication. This most recent method has been adopted for use here. For every vibrational band of each molecular contributor, it computes the maximum allowable rotational quantum number and is based on the shape of the Morse centrifugal potential that describes the rotating and vibrating molecule.

Further enhancements to the theory for the maximum rotational quantum number are possible, but this level of accuracy is sufficient for the current purpose.

Appendix C

Code Structure

Flowtrace Calling Tree Report

<u>Ordinal</u>	<u>Level</u>	<u>Routine name</u>
1	1	*SYSTEM
2	2	RMAIN
3	3	RADIAT
4	4	EVENLN
5	4	RDNONEQ
6	5	ASPECT
7	6	SORT
8	5	CONTN2
9	6	MUCONT
10	7	TAINT
11	6	MUMOL
12	5	EXCT
13	6	MDISSEQ
14	7	EQC
15	8	PARTM
16	6	MOLEXT
17	7	EQC (REPEAT to Tree Ordinal 14)
18	7	PARTM
19	7	PARTQ
20	8	PARTM
21	7	QSSM
22	8	ELECD
23	9	CROSAB
24	10	TAINT
25	8	EQC (REPEAT to Tree Ordinal 14)
26	8	EXCTML
27	9	AI3
28	10	SIMP
29	9	CROSAB (REPEAT to Tree Ordinal 23)
30	9	GAMC
31	9	GAMI
32	8	EXCTMM
33	8	PMINV
34	8	RATED
35	6	QSS
36	7	EONE
37	7	PMINV
38	5	LINT2
39	6	FREQ
40	6	MULE
41	5	MSPECT
42	6	CULL2
43	6	CULLER
44	6	MSORT
45	5	NODEN

46	6	PARTM
47	5	RADIN
48	6	MOLIN
49	7	JMAX
50	8	FKMAX
51	7	VMAX
52	8	FKMAX
53	5	SORT
54	4	SLABTR
55	5	TSFULL
56	6	TRNEQ
57	4	SUBGRD
58	5	TPD

Appendix D

Input Guide

Flow-Field, Control, and Line Inputs

Flow-Field Data: Nonuniform Condition Inputs

Below are the inputs for the flow field. This group contains the nonuniform condition inputs.

The following information is passed through the call statement to the radiation subroutine `rdnoneq`.

<code>etaln(k)</code>	array containing the normal coordinate of the grid points on the current normal line of the flow-field grid, cm
<code>tln(k), trln(k), tvln(k), teln(k)</code>	arrays containing respectively the heavy-particle translational, rotational, vibrational, and electron-electronic temperatures along the normal grid line, K
<code>(xnln(k,j), j=1,25)</code>	array containing the number densities in cm^{-3} of the radiating species along the normal grid line in the following order: N, O, C, H, Ar, N^+ , O^+ , C^+ , N^- , O^- , C^- , H^- , e^- , N_2 , O_2 , NO, C_2 , H_2 , CO, CN, C_3 , and N_2^+ , with three spares; the program can compute the number densities of the negative ions N^- , O^- , C^- , and H^- using a Saha equilibrium relation for these trace species; it also can compute an equilibrium number density of N_2^+ if no value is included for it
<code>kir</code>	k dimension of radiation subgrid along normal line
<code>ispct</code>	flag for optimized spectrum computation (initially set to 0; code sets to 1 after spectrum is computed)

Control Data

The following data are contained in file `radneq.in`. They are read into the program in subroutine `radin.f`. Generally, only the values on the first five cards in this input file must be changed unless a user has newer atomic line data. (Note that these inputs are called cards; in fact, they are simply lines in the input file. The terminology has been retained from the RAD/EQUIL code.)

Card 1, Format (f10.4)

Field 1, (Columns 1-10), tw

Wall temperature (K). Used in the radiative transport calculation. To obtain the incident radiation, this value should be set to zero so that the wall reradiation does not affect the result.

Card 2, Format (2f10.2)

Field 1, (Columns 6-15), wmin

Minimum frequency for the radiation computation (eV).

Field 2, (Columns 16-25), wmax

Maximum frequency for the radiation computation (eV).

Card 3, Format (20i1, 15a4)

Field 1, (Columns 1-20), kr

see description below

Field 2, (Columns 21-80), CASE

Title of the case (alphanumeric) used for identification of printed output.

Description of **kr** flags

Column 1	not used
Column 2	determines whether continuum radiation is included
0	include
1	do not include
Column 3	determines if molecules are to be included in the calculation
0	molecules can be included (see also the ncrc variable which overrides this control)
1	molecules are not included (regardless of what ncrc is)
Column 4	determines whether the line contributions are calculated
0	exclude lines
1	include lines
Column 5	determines whether equilibrium or nonequilibrium excited state populations are to be used
0	nonequilibrium
1	Boltzmann equilibrium
Column 6	determines accuracy of rotational partition function used
0	approximate
1	exact
Column 7	determines whether intensity or flux is to be calculated
0	intensity
1	flux

Column 8	determines whether frequency or wavelength is used in output
0	uses frequency, $h\nu$, eV
1	uses wavelength, λ , Å
Column 9	determines if the program is to check the validity of the continuum frequency grid (i.e., do the input spectral limits include at least 95 percent of the radiative energy?)
0	the grid is checked, use for energy transfer calculations
1	the grid is not checked, use when only a selected part of the spectrum is of interest
Column 10	determines whether incident or transmitted radiation is to be calculated
0	incident
1	transmitted
Column 11	determines whether tangent slab transport is used
0	nontangent slab
1	tangent slab
Column 12	determines atomic line shape used
0	Doppler/Lorentz
1	Voigt
Column 13	determines whether surface absorption and transmission properties are to be read in
0	not read in
1	read in
Columns 14 to 16	not used
Column 17	determines the amount of output
0	normal output
1	moderate output
2	extensive output
Columns 18 to 20	not used

Card 4, Format (24i3)

Field 1, (Columns 1-3, 4-6, etc.), nrc

Determine which radiation phenomena are to be included in the calculation and which are not. Flags for the species are given in the order shown in Table D.I, with meaning shown at right. Note that for the molecular species, the code is currently set up to include all bands or none. There is no provision to turn single molecular bands on and off from the input file. See the section on Input Files for a list of the molecular bands currently in LORAN.

Card 5, Format (6e12.8)

Field 1, (Columns 1-12), tob

Estimated maximum flowfield temperature (K), used to determine the necessary spectral region (see $kr(9)$) LORAN will also use the maximum temperature input in the Flowfield Data described previously.

Table DI. Radiation Phenomena Flags (See Card 4)

Index	Species	Flag for species
Atomic and ionic species		
1	N	0 → skip entirely 1 → bound free 2 → bound free + line 3 → bound free + free free 4 → bound free + free free + line (every atomic type) 5 → free free + line 6 → free free 7 → line
2	O	
3	C	
4	H	
5	Ar	
6	N ⁺	
7	O ⁺	
8	C ⁺	
9	N ⁻	
10	O ⁻	
11	C ⁻	
12	H ⁻	
Electron		
13	e^-	
Molecular species		
14	N ₂	0 → not included 1 → include through subroutine <code>mumol</code> (Smearred rotational line model)
15	O ₂	
16	NO	
17	C ₂	
18	H ₂	
19	CO	
20	CN	
21	C ₃	
22	N ₂ ⁺	

Line Data

Basic radiation data. This group is the atomic radiation database and should not be changed unless new species are added, new data become available, or a different treatment of multiplet lines is to be used. Special treatment is given to the four Lyman and Balmer α and β lines. Half-width information (a `gamp` value; see “Data on Line Transitions”) is read in for each of the remaining hydrogen lines. (Note that the half-width information for the Lyman γ and Paschen α lines is used to set up the frequency coordinate system only. For the lines which are still higher than these, the input `HWHM` is used throughout the transport calculation.) The hydrogen line calculation is from Nicolet’s work and has not been checked for the LORAN code. Therefore, the user should expect problems.

Card 1, Format (40i2)

Field 1, (Columns 1-2), nhv

Number of line groups to be included in the calculation (maximum of 25). A discussion of the judgments involved in selecting the appropriate number of line groups is given in the discussion of the *fhvm* and *fhvp* values.

Field 2, (Columns 5-6), nxi

This is the number of special hydrogen lines for which no HWHM data is read in. When the hydrogen lines are to be included, $nxi = 4$. Otherwise, it equals zero.

Line group specification.

Cards 1, 2...n1, Format (6e12.4)

Field 1, (Columns 1-12, 13-24, etc.), fhvm

Low frequency boundaries on the line groups. An *fhvm* value along with an *fhvp* value defines a frequency increment. All the lines with their centers within that increment define a line group. The continuum properties are evaluated at only one frequency point for each line in the line group. Contributions to the transport from sources outside the boundaries of the line group area are not taken into account. Therefore, the boundaries of a line group should never be too close to the center of a line within the group.

Cards n1+1, n1+2...n2, Format (6e12.4)

Field 1, (Columns 1-12, 13-24, etc.), fhvp

Corresponding high frequency boundaries on the line groups.

Cards n2+1, n2+2...n3, Format (6e12.4)

Field 1, (Columns 1-12, 13-24, etc.), fhv

Frequencies used to determine whether a line group falls within wmin and wmax. Usually taken to be roughly midway between *fhvm* and *fhvp*. Thus *fhv* is referred to as the “average” frequency of the line group.

Hydrogen index (skip this group if nxi = 0).

Card 1, Format (40i2)

Field 1, (Columns 1-2, 3-4, etc.), ia

Indices on the line groups which contain the special hydrogen lines (one per group, maximum). The line groups are always numbered sequentially starting with those at the lowest frequency. (The calculation of hydrogen lines is from RAD/EQUIL and has not been checked out in LORAN.)

Number of lines per line group.

Card 1, Format (40i2)

Field 1, (Columns 1-2, 3-4, etc.), nu

Number of lines in each line group to be treated individually. Must equal the number of line data cards read in for each group. Whenever a line is incorrectly assigned to a line group the program will stop and write out the message “LINE CENTER OUT OF GROUP FREQUENCY RANGE.”

Data on line transitions.

Cards 1,2...no. of lines, Format (i2,1x,i2,2e12.1,3e12.2,f5.1,f7.3)

Fields 1-9, nd, nup, hvl, ff, gamp, xnol, gup, gl, el

see descriptions below

Table DII. Index of Radiating Species and Level

Index	Species
1-22	N
23-41	O
42-49	C
50-57	H
58-65	Ar
66-73	N ⁺
74-81	O ⁺
82-89	C ⁺

- Field 1 (columns 1-2), **nd** index of the lower (absorbing) level of the line; identifies the radiating atomic and ionic species and level according to the scheme in table DII where the index increases (for each species) with increasing energy level
- Field 2 (columns 4-5), **nup** index of the upper (emitting) level of the line
- Field 3 (columns 6-17), **hvl** frequency of the center of the line, eV
- Field 4 (columns 18-29), **ff** f-number of the line when the lower level of the transition is unlumped; when it is lumped, $\mathbf{ff} = (\mathbf{gee} * \mathbf{f}) / \mathbf{gee}$ (sum over lumped), where **gee** is the statistical weight of the unlumped lower level of the transition
- Field 5 (columns 30-41), **gamp** HWHM per free electron due to Stark broadening, evaluated at 10 000 K (see ref. 3)
- Field 6 (columns 42-53), **xno1** number of lines in a given line group which have identical properties; it is used only when multiplet-averaged lines are included; spectral properties are calculated for the averaged line; the line width is then multiplied by the number of original lines to obtain the effective total; only lines in the low-frequency region (roughly less than 5 eV) should be averaged in this manner; in cases where approximate results are sufficient, high-frequency lines may be multiplet-averaged as well
- Field 7 (columns 54-65), **gup** statistical weight of the upper level of the line (used in resonance broadening calculation only)
- Field 8 (columns 66-70), **gl** statistical weight of the lower level of the line
- Field 9 (columns 71-77), **e1** energy level of the lower state of the line transition, eV

Surface Absorptivity/Emissivity and Transmissivity Data

Skip this input deck if **kr**(13) \neq 1.

Card Set 1, Free Format

Fields 1 through nabtr, fabtr(j)

Frequencies at which surface properties are given (eV)

Card Set 2, Free Format

Fields 1 through nabtr, ahv(j)

Surface absorptivity/emissivity at corresponding frequency

Card Set 3, Free Format

Fields 1 through nabtr, tmsw(j)

Surface transmissivity at corresponding frequency

NEQAIR Excitation and Radiation Inputs

The following data are contained in file `neq.in`. They are read into the program in subroutines `radin.f` and `molin.f`. Note that all inputs are in cm^{-1} for consistency with the NEQAIR code, but the inputs are immediately converted to electron volts within the code.

Atomic Data

This excitation database for atoms will not change unless the user has new data, new models, or new species. These data must be included for each atomic species in the radiation calculation.

Energy level data.

Card 1, Format (1x,2a4,1x,g10.3)

Fields 1-2, (Columns 2-9), atomx

Atomic species name.

Field 3, (Columns 11-20), eiona

Ionization potential of the corresponding ion (1/cm).

Card 2, Format (8g10.3)

Fields 1-4, (Columns 1-40), gp

Degeneracies of the first four electronic states of the corresponding ion.

Fields 5-8, (Columns 41-80), ep

Energy levels of the first four electronic states of the corresponding ion (1/cm).

Card set 3, Format (2i5,2g10.3)

Field 1, (Columns 1-5), me

Index of the electronic level.

Field 2, (Columns 6-10), npr

Principal quantum number of the electronic level.

Field 3, (Columns 11-20), elev

Energy level of the electronic state (1/cm).

Field 4, (Columns 21-30), stwt

Degeneracy of the electronic state.

Transition data.

Card set 1, Format (2i5,2g10.3)

Field 1, (Columns 1-5), jl

Index of lower level.

Field 2, (Columns 6-10), ju

Index of upper level.

Field 3, (Columns 11-20), al

Optical transition rate.

Card set 2, Format (i10,2g10.3)

Field 1, (Columns 1-10), jp

Index of level.

Field 2, (Columns 11-20), cz

Constant multiplier in expression for continuum absorption coefficient.

Field 3, (Columns 21-30), anz

Exponent in expression for continuum absorption coefficient.

Card set 3, Format (4(2i3,1pg8.1,0pf5.2))

The following fields repeat across and down this card set.

Field 1, (Columns 1-3), j1

Index of lower electronic level.

Field 2, (Columns 4-6), k1

Index of upper electronic level.

Field 3, (Columns 7-14), a1

Constant multiplier in expression for excitation rate between two levels.

Field 4, (Columns 15-19), e1

Exponent in expression for excitation rate between two levels.

Molecular Radiation Data

The following inputs are used in the radiation calculation portion of the LORAN code and are the properties for radiating transitions. This database should be changed only if new data become available or new species are added. These data must be included for each molecular band in the radiation calculation.

Card 1, Format (1x,2a3,3x,f10.3,4i5)

Field 1-2, (Columns 2-7), amol(1-2,ib)

Name of band.

Field 3, (Columns 11-20), aw(ib)

Molecular weight of species, (g/mol).

Field 4, (Columns 21-25), lmol(1,ib)

Type index of molecular band.

Field 5, (Columns 26-30), lmol(2,ib)

Number of bands.

Field 6, (Columns 31-35), lmol(3,ib)

Number of energy levels.

Field 7, (Columns 36-40), lmol(4,ib)

Symmetry factor for heteronuclear (1) and homonuclear (2) molecules.

Card 2, Format (i10,7g10.3)

Field 1, (Columns 1-10), lmol(3,ib)

As above

Field 2, (Columns 11-20), sp(2,1,ib)

Alternating line strength factor (not used).

Field 3, (Columns 21-30), sp(3,1,ib)

Dissociation energy of state (1/cm).

Field 4, (Columns 31-40), sp(4,1,ib)

Morse potential constant β (1/cm).

Field 5, (Columns 41-50), sp(5,1,ib)

Equilibrium internuclear separation distance (A).

Field 6, (Columns 51-60), sp(6,1,ib)

Dissociation energy including zero point vibrational energy (1/cm).

Field 7, (Columns 61-70), sp(7,1,ib)

A , a higher order energy level correction (not used) (1/cm).

Field 8, (Columns 71-80), sp(8,1,ib)

Angular momentum quantum number (not used).

Card 3, Format (8g10.3)

Same as Card 2 for the upper state of the band (with 2nd index=2) except.

Field 1, (Columns 1-10), sp(1,2,ib)

Reduced mass of molecule (g/mol).

Card 4, Format (8g10.3)

Field 1, (Columns 1-10), sp(1,3,ib)

Degeneracy of lower electronic state of band.

Field 2, (Columns 11-20), sp(2,3,ib)

Energy level of lower electronic state of band (1/cm).

Field 3, (Columns 21-30), sp(3,3,ib)

Spectroscopic constant ω_e of lower state of band (1/cm).

Field 4, (Columns 31-40), sp(4,3,ib)

Spectroscopic constant $\omega_e x_e$ of lower state of band (1/cm).

Field 5, (Columns 41-50), sp(5,3,ib)

Spectroscopic constant $\omega_e y_e$ of lower state of band (1/cm).

Field 6, (Columns 51-60), sp(6,3,ib)

Spectroscopic constant $\omega_e z_e$ of lower state of band (1/cm).

Field 7, (Columns 61-70), sp(7,3,ib)

Spectroscopic constant b_e of lower state of band (1/cm).

Field 8, (Columns 71-80), sp(8,3,ib)

Spectroscopic constant α_e of lower state of band (1/cm).

Card 5, Format (8g10.3)

Same as Card 4 for the upper state of the band (with 2nd index=4).

Card 6, Format (2f5.1,2g10.3,i5)

Field 1, (Columns 1-5), vib (1,j,ib)

Vibrational quantum number of upper state of vibrational transition.

Field 2, (Columns 6-10), vib (2,j,ib)

Vibrational quantum number of lower state of vibrational transition.

Field 3, (Columns 11-20), vib (3,j,ib)

Average value of the sum of the squares of the intermolecular distance r_e for the vibrational transition.

Field 4, (Columns 21-30), vib (4,j,ib)

Franck-Condon factor for the vibrational transition.

Field 5, (Columns 31-35), ka (j,ib)

Maximum rotational quantum number for the vibrational transition.

Card 6 is repeated for each vibrational transition considered.

Molecular Excitation Data

The following inputs are used in the excitation calculation portion of the LORAN code and are the properties for all excited states required to obtain populations for those excited states which radiate. This database should be changed only if new data or species are available or if new excitation models require testing. These data must be included for each molecular species treated in the LORAN code.

Card 1, Format (1x,2a3,3x,f10.3,6i5)

Fields 1-2, (Columns 2-7), amolec(1-2,is)

Name of molecular species

Field 3, (Columns 11-20), awb(is)

Molecular weight of species.

Field 4, (Columns 21-25), lmolec(1,is)

Number of electron-impact dissociation cross-section data sets (maximum 4 allowed).

Field 5, (Columns 26-30), lmolec(2,is)

Number of electron-impact excitation cross-section data sets (maximum 6 allowed).

Field 6, (Columns 31-35), lmolec(3,is)

Number of energy levels (maximum 8 allowed).

Field 7, (Columns 36-40), lmolec(4,is)

Number of first few electronic levels for which quasi-steady-state calculation is made (maximum 4 allowed).

Field 8, (Columns 41-45), lmolec(5,is)

Symmetry factor (1=hetero, 2=homonuclear).

Card set 2, Format (8g10.3)

Field 1, (Columns 1-10), spec2(1,jn,is)

Electronic degeneracy of state jn .

Field 2, (Columns 11-20), spec2(2,jn,is)

Energy level of state jn (1/cm).

Field 3, (Columns 21-30), spec2(3,jn,is)

Spectroscopic constant ω_e of state jn (1/cm).

Field 4, (Columns 31-40), spec2(4,jn,is)

Spectroscopic constant $\omega_e x_e$ of state jn (1/cm).

Field 5, (Columns 41-50), spec2(5,jn,is)

Spectroscopic constant $\omega_e y_e$ of state jn (1/cm).

Field 6, (Columns 51-60), spec2(6,jn,is)

Spectroscopic constant $\omega_e z_e$ of state jn (1/cm).

Field 7, (Columns 61-70), spec2(7,jn,is)

Spectroscopic constant b_e of state jn (1/cm).

Field 8, (Columns 71-80), spec2(8,jn,is)

Spectroscopic constant α_e of state jn (1/cm).

Field 9, (Columns 81-90), spec2(9,jn,is)

Equilibrium internuclear separation r_e (Angstroms)

Field 10, (Columns 91-100), spec2(10,jn,is)

Dissociation energy D_0 (1/cm).

Field 11, (Columns 101-110), spec2(11,jn,is)

Rotational spectroscopic constant D_e (1/cm).

Field 12, (Columns 111-120), spec2(12,jn,is)

Second rotational spectroscopic constant β_e (1/cm).

Card 2 is repeated for each energy level to be included for the molecule.

Card 3, Format (1x,2a3,3x,7g10.3)

Field 1-2, (Columns 2-7), atom(1-2,1,is)

First dissociated atom created from this molecular species.

Field 3, (Columns 11-20), atw(1,1,is)

Atomic weight of atom

Field 4, (Columns 21-30), atw(2,1,is)

Dissociation energy for the molecule (1/cm).

Field 5, (Columns 31-40), atw(3,1,is)

Degeneracy (statistical weight) of ground state of atom.

Card 4, Format (1x,2a3,3x,7g10.3)

The above information is repeated for the second dissociated atomic species.

Card 5, Format (20a4)

Field 1, (Columns 1-80), title

Information concerning the source of the dissociation cross-sections which follow.

Card 6, Format (8g10.3)

Field 1, (Columns 1-10), edis(it,is)

Dissociation energy of *it*-th electronic state (1/cm).

Card 7, Format (8g10.3)

Field 1, (Columns 1-10, 11-20, etc.), *ed*

Electron energy for dissociation cross-section (1/cm).

Card 8, Format (8g10.3)

Field 1, (Columns 1-10, 11-20, etc.), *sigmd*

Cross-sections for dissociation at energy *ed* (cm²).

Cards 5-8 are repeated for each set of dissociation cross sections.

Card 9, Format (1x,2a3,3x,3i5)

Field 1, (Columns 2-4), *spell1*

Lower state of molecular transition.

Field 2, (Columns 5-7), *spell2*

Upper state of molecular transition.

Field 3-4, (Columns 11-20), *ilst(1-2,it,is)*

Lower and upper electronic state index (*it*=transition number in a molecule).

Field 5, (Columns 21-25), *ncard*

Number of cards of Franck-Condon factor data which follow.

Card set 10, Format (5(2i3,g10.3))

The following fields repeat across and down this card set.

Field 1, (Columns 1-3), $j1$

Lower state index.

Field 2, (Columns 4-6), $j2$

Upper state index.

Field 3, (Columns 7-16), $f1$

Franck-Condon factor for the transition between states $j1$ and $j2$.

Card 11, Format (20a4)

Field 1, (Columns 1-80), title

Information concerning the source of the electron-impact excitation cross-sections which follow.

Card 12, Format (8g10.3)

Field 1, (Columns 1-10, 11-20, etc.), ee

Electron energy for electron-impact excitation cross-section (1/cm).

Card 13, Format (8g10.3)

Field 1, (Columns 1-10, 11-20, etc.), sigma

Cross-sections for electron-impact excitation at energy ee (cm^2).

Card 14, Format (8g10.3)

Field 1, (Columns 1-10), arad(mu,ml,is)

Radiative transition probability for the transition from level mu to ml .

Cards 9–14 are repeated for each transition considered.

Appendix E

Tecplot File Format

The Tecplot output produced by the LORAN code consists of both I- and IJ-ordered files. Each file starts with a variables declaration of the form shown in the first line of table EI. The second line contains information about the size of the file and the order of the data. In table EI, **imax** is the size of the I-ordered data set. If the optional **jmax** is included, it implies an IJ-ordered data set and gives a second dimension. The term **orderformat** is an optional variable indicating the data layout. When excluded, each column in the file corresponds to a variable. When set to block, each row of data corresponds to a variable (multiple rows will appear for each variable when the data set dimensions are large). Data for the zone then follow and are ordered according to **orderformat** and whether the file is I or IJ ordered.

Additional zones of data can be included in the same file (for example, the variables along each normal grid line can be included as separate zones), as shown in table EI.

Table EI. Tecplot File Format

```
VARIABLES = vname1, vname2, ...
ZONE I = imax, [J = jmax,] [F = orderformat]
Data for ordered zone

ZONE I = imax, [J = jmax,] [F = orderformat]
Data for ordered zone

etc
```

References

1. Park, Chul: *Nonequilibrium Air Radiation (NEQAIR) Program: User's Manual*. NASA TM-86707, 1985.
2. Nicolet, William E.: *Advanced Methods for Calculating Radiation Transport in Ablation-Product Contaminated Boundary Layers*. NASA CR-1656, 1970.
3. Griem, Hans R.: *Spectral Line Broadening by Plasmas*. Academic Press, 1974.
4. Page, William A.; Compton, Dale L.; Borucki, William J.; Ciffone, Donald L.; and Cooper, David M.: Radiative Transport in Inviscid Non-Adiabatic Stagnation-Region Shock Layers. AIAA-68-784, 1968.
5. Hunt, Brian L.; and Sibulkin, Merwin: *Radiative Transfer in a Gas of Uniform Properties in Local Thermodynamic Equilibrium*, Parts 1-3. Rep. Nos. Nonr-562(35)/16-18, U. S. Navy, Dec. 1966. (Available from DTIC as AD 648 398-AD 648 400.)
6. Bond, John W., Jr.; Watson, Kenneth M.; and Welch, Jasper A., Jr.: *Atomic Theory of Gas Dynamics*. Addison-Wesley Publ. Co., Inc., 1965.
7. Whiting, E. E.: An Empirical Approximation to the Voigt Profile. *J. Quant. Spectrosc. & Radiat. Transf.*, vol. 8, no. 6, June 1968, pp. 1379-1384.
8. Olivero, J. J.; and Longbothum, R. L.: Empirical Fits to the Voigt Line Width: A Brief Review. *J. Quant. Spectrosc. Radiat. Transf.*, vol. 17, 1977, pp. 233-236.
9. Zeldovich, I. A. B.; and Raizer, Yu. P.: *Physics of Shock Waves and High-Temperature Hydrodynamic Phenomena*. Wallace D. Hayes and Ronald F. Probstein, eds., (Scripta Technica., transl.), Academic Press, 1967.
10. Biberman, L. M.: Recombination Radiation and Bremsstrahlung of a Plasma. *J. Quant. Spectrosc. & Radiat. Transf.*, vol. 3, 1963, pp. 221-245.
11. Penner, S. S.: *Quantitative Molecular Spectroscopy and Gas Emissivities*. Addison-Wesley Publ. Co., Inc., 1959.
12. Patch, R. W.; Shackleford, W. L.; and Penner, S. S.: Approximate Spectral Absorption Coefficient Calculations for Electronic Band Systems Belonging to Diatomic Molecules. *J. Quant. Spectrosc. & Radiat. Transf.*, vol. 2, July-Sept. 1962, pp. 263-271.
13. Herzberg, Gerhard: *Molecular Spectra and Molecular Structure. I. Spectra of Diatomic Molecules*, Second ed. D. Van Nostrand Co., Inc., 1950.
14. Park, Chul: *Nonequilibrium Hypersonic Aerothermodynamics*. John Wiley & Sons, Inc., 1990.
15. Park, Chul: Hydrogen Line Ratios as Electron Temperature Indicators in Nonequilibrium Plasmas. *J. Quant. Spectrosc. & Radiat. Transf.*, vol. 12, Mar. 1972, pp. 323-370.
16. Park, Chul: Comparison of Electron and Electronic Temperatures in Recombining Nozzle Flow of Ionized Nitrogen-Hydrogen Mixture. Part 1. Theory. *J. Plasma Phys.*, vol. 9, pt. 2, 1973, pp. 187-215.
17. Ozisik, M. Necati: *Radiative Transfer and Interactions With Conduction and Convection*. John Wiley & Sons, Inc., 1973.
18. Hartung, Lin C.; and Hassan, H. A.: Radiation Transport Around Axisymmetric Blunt Body Vehicles Using a Modified Differential Approximation. *J. Thermophys. & Heat Transf.*, vol. 7, no. 2, Apr.-June 1993, pp. 220-227.
19. Gnoffo, Peter A.; Gupta, Roop N.; and Shinn, Judy L.: *Conservation Equations and Physical Models for Hypersonic Air Flows in Thermal and Chemical Nonequilibrium*. NASA TP-2867, 1989.
20. Park, Chul: Assessment of Two-Temperature Kinetic Model for Ionizing Air. *J. Thermophys.*, vol. 3, no. 3, July 1989, pp. 233-244.
21. Nicolet, W. E.: *User's Manual for the Generalized Radiation Transfer Code (RAD/EQUIL)*. NASA CR-116353, 1969.
22. Gnoffo, Peter A.: Point-Implicit Relaxation Strategies for Viscous, Hypersonic Flows. *Computational Methods in Hypersonic Aerodynamics*, Mech. Publ./Kluwer Acad. Publ., 1992, pp. 115-151.
23. Sharma, Surendra P.; Gillespie, Walter D.; and Meyer, Scott A.: Shock Front Radiation Measurements in Air. AIAA-91-0573, Jan. 1991.
24. Taylor, Jeff C.; Carlson, Ann B.; and Hassan, H. A.: Monte Carlo Simulation of Radiating Reentry Flows. AIAA-93-2809, July 1993.

25. Olynick, David R.: A New LU-SGS Flow Solver For Calculating Reentry Flows. Ph.D. Diss., North Carolina State University, 1992.
26. Olynick, David R.; Henline, W. D.; Chambers, Lin Hartung; and Candler, G. V.: Comparison of Coupled Radiative Navier-Stokes Flow Solutions With the Project Fire II Flight Data. AIAA-94-1955, 1994.
27. Wiese, W. L.; Smith, M. W.; and Glennon, B. M.: Atomic Transition Probabilities. Volume 1— Hydrogen Through Neon, U. S. Dep. Commerce, NSRDS-NBS 4, May 20, 1966.
28. Park, C.: Calculation of Radiation From Argon Shock Layers. *J. Quant. Spectrosc. & Radiat. Transf.*, vol. 28, July 1982, pp. 29–40.
29. Anderson, Dale A.; Tannehill, John C.; and Pletcher, Richard H.: *Computational Fluid Mechanics and Heat Transfer*. Hemisphere Publ. Corp., 1984.
30. Park, Chul; and Milos, Frank S.: Computational Equations for Radiating and Ablating Shock Layers. AIAA-90-0356, Jan. 1990.
31. Gnoffo, Peter A.; Hartung, Lin C.; and Greedyke, Robert B.: Heating Analysis for a Lunar Transfer Vehicle at Near-Equilibrium Flow Conditions. AIAA-93-0270, Jan. 1993.
32. Stanley, Scott A.; and Carlson, Leland A.: The Effects of Shock Wave Precursors Ahead of Hypersonic Entry Vehicles. AIAA-91-1465, June 1991.
33. Hartung, Lin C.: Development of a Nonequilibrium Radiative Heating Prediction Method for Coupled Flowfield Solutions. AIAA-91-1406, June 1991.
34. Bolz, Charles W., Jr.: *An Algorithm for Selecting a Radiation Transport Subgrid for Ablation and Radiation Coupled Hypersonic Viscous-Shock-Layer Problems*. NASA CR-144957, 1976.
35. Hartung, Lin C.: *Nonequilibrium Radiative Heating Prediction Method for Aeroassist Flowfields With Coupling to Flowfield Solvers*. Ph.D. Diss., North Carolina State Univ., Apr. 1991. (Also available as NASA CR-188112, 1991.)
36. Hartung, Lin C.; Mitcheltree, Robert A.; and Gnoffo, Peter A.: Stagnation Point Nonequilibrium Radiative Heating and the Influence of Energy Exchange Models. *J. Thermophys. & Heat Transf.*, vol. 6, no. 3, July–Sept. 1992, pp. 412–418.
37. Hartung, Lin C.; Mitcheltree, Robert A.; and Gnoffo, Peter A.: Coupled Radiation Effects in Thermochemical Nonequilibrium Shock-Capturing Flowfield Calculations. *J. Thermophys. & Heat Transf.*, vol. 8, no. 2, Apr.–June 1994, pp. 244–250.
38. Greedyke, Robert B.; and Hartung, Lin C.: A Convection and Radiative Heat Transfer Analysis for the Fire II Forebody. AIAA-93-3194, July 1993.
39. *TecplotTM—Version 6, User's Manual*. Amtec Eng., Inc., 1993.
40. Vincenti, Walter G.; and Kruger, Charles H., Jr.: *Introduction to Physical Gas Dynamics*. Robert E. Krieger Publ. Co., Inc., 1982.
41. Whiting, Ellis E.; Arnold, James O.; and Lyle, Gilbert C.: *A Computer Program for a Line-by-Line Calculation of Spectra From Diatomic Molecules and Atoms Assuming a Voigt Line Profile*. NASA TN D-5088, 1969.

REPORT DOCUMENTATION PAGE			Form Approved OMB No. 0704-0188	
Public reporting burden for this collection of information is estimated to average 1 hour per response, including the time for reviewing instructions, searching existing data sources, gathering and maintaining the data needed, and completing and reviewing the collection of information. Send comments regarding this burden estimate or any other aspect of this collection of information, including suggestions for reducing this burden, to Washington Headquarters Services, Directorate for Information Operations and Reports, 1215 Jefferson Davis Highway, Suite 1204, Arlington, VA 22202-4302, and to the Office of Management and Budget, Paperwork Reduction Project (0704-0188), Washington, DC 20503.				
1. AGENCY USE ONLY (Leave blank)	2. REPORT DATE September 1994	3. REPORT TYPE AND DATES COVERED Technical Memorandum		
4. TITLE AND SUBTITLE Predicting Radiative Heat Transfer in Thermochemical Nonequilibrium Flow Fields <i>Theory and User's Manual for the LORAN Code</i>			5. FUNDING NUMBERS WU 506-40-91-01	
6. AUTHOR(S) Lin Hartung Chambers				
7. PERFORMING ORGANIZATION NAME(S) AND ADDRESS(ES) NASA Langley Research Center Hampton, VA 23681-0001			8. PERFORMING ORGANIZATION REPORT NUMBER L-17372	
9. SPONSORING/MONITORING AGENCY NAME(S) AND ADDRESS(ES) National Aeronautics and Space Administration Washington, DC 20546-0001			10. SPONSORING/MONITORING AGENCY REPORT NUMBER NASA TM-4564	
11. SUPPLEMENTARY NOTES Part of the information in this report was included in a thesis submitted by Lin C. Hartung in partial fulfillment of the requirements for the Degree of Doctor of Philosophy in Aerospace Engineering, North Carolina State University, Raleigh, North Carolina, April 1991.				
12a. DISTRIBUTION/AVAILABILITY STATEMENT Unclassified-Unlimited Subject Category 34			12b. DISTRIBUTION CODE	
13. ABSTRACT (Maximum 200 words) The theory for radiation emission, absorption, and transfer in a thermochemical nonequilibrium flow is presented. The expressions developed reduce correctly to the limit at equilibrium. To implement the theory in a practical computer code, some approximations are used, particularly the smearing of molecular radiation. Details of these approximations are presented and helpful information is included concerning the use of the computer code. This user's manual should benefit both occasional users of the Langley Optimized Radiative Nonequilibrium (LORAN) code and those who wish to use it to experiment with improved models or properties.				
14. SUBJECT TERMS Radiative heat transfer; Thermochemical nonequilibrium; Radiative coupling			15. NUMBER OF PAGES 72	
			16. PRICE CODE A04	
17. SECURITY CLASSIFICATION OF REPORT Unclassified	18. SECURITY CLASSIFICATION OF THIS PAGE Unclassified	19. SECURITY CLASSIFICATION OF ABSTRACT Unclassified	20. LIMITATION OF ABSTRACT	